Macromodel Order Reduction and Passivity Enforcement using Hamiltonian Matrix Pencil Perturbation

Marco T. Kassis

Master of Engineering

Department of Electrical and Computer Engineering

McGill University

Montréal, Québec

2015-10-07

A thesis submitted to McGill University in partial fulfillment of the requirements of the degree of Master of Engineering in Electrical Engineering

DEDICATION

To Athanasius and George, thank you!

ACKNOWLEDGMENTS

First and foremost, I would like to thank my supervisor Prof. Roni Khazaka, who has been constantly and continuously providing me with guidance and knowledge that has made my whole Master of Engineering experience enlightening. Very extensive thanks go to Muhammad Kabir for his priceless support in all my research work. I would love to extend my thanks to our whole research group by name, Marwan Kanaan, Julian Santorelli, Yi Qing Xiao and Zhaoqing Liu for their enriching discussions and continuous help.

Special thanks go to my best friends Ahmed Khorshid, Nassir Abou Ziki, Raffi Toukhtarian, Mohamed Leila, Hassana El-Zein, Martine Chlela and Michelle Mekary for making this an unforgettable journey and for their words of encouragement. Special acknowledgments go to Prof. Sourajeet Roy and his research group for hosting me in Collorado State University, which broadened my horizons and expanded my research work positively.

Last but definitely not least, very heartfelt thanks go to my whole family, especially my father, Tony Kassis, my mother, Suzan Attallah, and my brother, Michel Kassis, for being my invaluable source of power throughout the years, even remotely. I will be forever indebted to all their help and motivating words.

ABSTRACT

Model Order Reduction is one of the most successful methods to minimize computational complexity in circuit simulation. Order reduction could be done as a part of the macromodeling process of frequency domain data into a highly accurate and compact time domain model. This macromodeling is done by converting the frequency domain Y-parameter or S-parameter data, which were extracted using full-wave simulation of the physical model at hand, into a descriptor state space based time domain model. Using the system identification method of Loewner Matrix, the order selection process can only be done to a certain threshold, below which a non-passive model would be produced. Such a non-passive model could become unstable when connected to other terminations, even if such terminations are stable themselves. This thesis presents a novel approach of utilizing passivity enforcement schemes, such as Hamiltonian Matrix Pencil Perturbation, to convert a system with mild passivity violation into a passive system. This would allow the macromodeling process to use an order lower than the minimum threshold, making order reduction much more efficient and effective. This whole methodology can be used to create compact time domain macromodels for the recently popular microwave applications, which otherwise would be difficult, or impossible, to find their closed form expressions using their physics based information.

ABRÉGÉ

Le modèle de réduction de séquence est une des méthodes les plus réussites afin de réduire au maximum la complexité computationnel en simulation de circuit. La réduction de séquence pourrait être faite dans le cadre du processus de macromodélisation de données du domaine des fréquences dans le modèle de domaine temporel extrêmement exact, précis et compact. Cette macromodélisation est faite en convertissant le paramètre-Y ou le paramètre-S des données du domaine des fréquences, qui on été extraites en utilisant la simulation à deux alternances du modèle physique à portée de mains, dans l'état descripteur du modèle de domaine d'espace-temps. Utilisant la méthode d'identification du système de Loewner Matrix, le processus de sélection de commande peut être fait qu'à un certain seuil, en dessous duquel un modèle non passif serait produit. Un tel modèle non passif pourrait devenir instable lorsque connecté à d'autre terminaisons, même si ces terminaisons sont stables eux-mêmes. Cette mémoire de maitrise présente une nouvelle approche de l'utilisation des schémas d'applications de passivité, tel que la perturbation du faisceau de matrices hamiltonienne, afin de convertir un système avec une légère violation de passivité dans un système passif. Cela permettrait au processus de macromodélisation d'utiliser une commande inférieure au seuil minimum, faisant de la réduction de séquence beaucoup plus efficace. Toute cette méthodologie peut être utilisée afin de créer un macromodèle compact du domaine temporel pour l'utilisation des récentes applications de micro-ondes, qui serait difficiles autrement,

voire impossible, de trouver leur expression en forme analytique utilisant leur informations basées sur la physique.

TABLE OF CONTENTS

DEDICATION ii

ACKNOWLEDGMENTS iii

ABSTRACT iv

ABRÉGÉ v

LIST OF TABLES ix

LIST OF FIGURES x

1 Introduction 1

2 Literature Review 3

2.1 System Identification Tools 4
2.1.1 Least-Squares Approximations 4
2.1.2 Vector Fitting 6
2.1.3 Loewner Matrix 9
2.2 Passivity and Passivity Enforcement 16

3 Thesis Contribution 20

3.1 Loewner Matrix 20
3.2 Passivity Checking 20
3.3 Order Reduction 26
3.3.1 Finding Minimal Passive Order 26
3.3.2 Reducing Order Further till Maximum Rectifiable Passivity Violation 31
3.3.3 Determining Purely Imaginary Eigenvalues of $(\mathcal{J}, \mathcal{K})$ 31
3.4 Passivity Enforcement 35
3.4.1 Model Conversion 36
3.4.2 Impulse Checking 37

3.4.3 Proper Part Perturbation 39
3.5 SPICE Netlist Generation 45

4 Implementation Examples 47

4.1 Example 1: 8-Traces Microstrip Line 48
4.1.1 Correctness Validation 48
4.1.2 Accuracy Validation 49
4.2 Example 2: 16-Traces Microstrip Line 53
4.2.1 Correctness Validation 53
4.2.2 Accuracy Validation 54

5 Conclusion 58

References 61

LIST OF TABLES

Table page

5–1 Examples Parameters and Characteristics Summary 59

5–2 Examples Error Summary 59

LIST OF FIGURES

Figure		page
2–1	N-Line S-Parameter System with Incident and Reflected Power Waves	10
3–1	Arbitrary Generalized Eigenvalues of $(\mathcal{J}, \mathcal{K})$ Matrix Pencil	24
3–2	Maximum singular values of sample S-parameter matrices with and without a passivity violation	25
3–3	Sample S-parameter Data for a Lumped System	27
3–4	Sample Singular Value Decomposition for Lumped System	27
3–5	Sample S-parameter Data for a Distributed System	28
3–6	Sample Singular Value Decomposition for Distributed System	28
3–7	Sample Pairing and Non-Pairing Eigenvalues of $(\mathcal{J}, \mathcal{K})$ Matrix Pencil	33
3–8	Equivalent Voltage-Current Realization of Terminal Power Wave Representations	46
4–1	Microstrip line structure	47
4–2	Maximum Singular Values of Example 1's S-Parameter Matrices Before and After Passivity Enforcement	48
4–3	Magnified Maximum Singular Values of Example 1's S-Parameter Matrices Before and After Passivity Enforcement	49
4–4	RMS Error Across Frequency Spectrum for Example 1	50
4–5	Magnitude of Aggressor Line Response at $(10, 10)$ for Example 1	51
4–6	Phase of Aggressor Line Response at $(10, 10)$ for Example 1	51
4–7	Magnitude of Victim Line Response at $(2, 16)$ for Example 1	52

4–8 Phase of Victim Line Response at $(2, 16)$ for Example 1 52

4–9 Maximum Singular Values of Example 2's S-Parameter Matrices Before and After Passivity Enforcement 54

4–10 Magnified Maximum Singular Values of Example 2's S-Parameter Matrices Before and After Passivity Enforcement 55

4–11 RMS Error Across Frequency Spectrum for Example 2 55

4–12 Magnitude of Aggressor Line Response at $(4, 4)$ for Example 2 56

4–13 Phase of Aggressor Line Response at $(4, 4)$ for Example 2 56

4–14 Magnitude of Victim Line Response at $(8, 12)$ for Example 2 57

4–15 Phase of Victim Line Response at $(8, 12)$ for Example 2 57

CHAPTER 1
Introduction

The challenge of analytically retrieving an accurate physics based model for complex multiport linear structures is becoming much more prominent nowadays in several microwave applications. In order to get over such a problem, accurate frequency domain representations have been generated, such as Y-parameters and S-parameters, which are achieved by full-wave simulations and fully describe such structures within two boundary frequency points, f_{start} and f_{end}. This is then followed by measurement based macromodeling techniques, such as Least-Squares Approximations method [6], Vector Fitting [9, 10, 5, 26] and Loewner Matrix method [25, 19, 32, 12, 17]. Such tools have become very popular in producing a compact time domain macromodel, that matches the original frequency domain data with high accuracy and is also SPICE compatible, for universal compatibility of the output.

The Loewner Matrix method produces macromodels that have high accuracy [12]. Such a high accuracy could be unnecessary for certain applications, hence order reduction can be done which would result in a more compact final model, and hence a smaller SPICE netlist, which would significantly reduce computational complexity and computational time of the simulation process. Hence, when the macromodeling process is being done, order selection of a smaller order could be done, however, the main problem that could be faced is that after selecting an order

lower than a certain threshold m_{min}, the system could start demonstrating non-passive behavior. Such passivity violation could greatly compromise the stability of the system when connected to other terminations, even if both components are stable, after the macromodel has been extracted.

In order to avoid problems with stability with the final model, the selected order can either be higher than m_{min}, or a passivity enforcement scheme can be used to rectify the passivity violation resulting from selecting an order less than m_{min}. The latter option is the one presented in this thesis, in which Hamiltonian Matrix Pencil Perturbation method [33, 34] is used to rectify a mildly non-passive region within the frequency spectrum of the model at hand. This eventually generates a highly accurate, much reduced, stable and passive time domain macromodel that correctly matches the original frequency domain data.

This thesis starts with a literature review of all the basic concepts related to or used in the works presented and comparing them to each other, such as the different system identification methods, as well the physical definitions of passivity. This is then followed by a detailed description of the whole process starting with macro-modeling the frequency domain data, followed by checking the passivity conditions of the model [38, 1], then the process of order reduction [18, 16], then finally the passivity enforcement scheme utilized [34]. A procedure of how the data can then be converted into a SPICE compatible netlist is then presented as shown in [16]. Finally, two microstrip line examples, based on [18], are shown with all their results, which serve as successful applications of the contributions of this thesis.

CHAPTER 2
Literature Review

This chapter presents a brief review of the existing theory behind which the work presented in this thesis is built. In many of the contemporary microwave and high-frequency applications, complex multiport linear structures with hard-to-attain accurate physics-based analytical models have become very common. These models would generally be formulated as first-order differential equations suitable for circuit simulation. However, one can usually obtain accurate frequency-domain data such as S or Y-parameter data, which describe such structures via measurements or full-wave simulation tools.

System Identification Tools are hence needed to help macromodel such frequency-domain data and convert them into a time-domain rational approximation which is needed for circuit simulations. Such System Identification Methods include Least-Squares Approximations, Vector Fitting and Loewner Matrix Method, which are discussed in the first section of this chapter.

The scope of this thesis is to produce reduced order macromodels, to make use of all the inherent benefits of order reduction such as better memory usage and less computational expenditure when simulating the produced macromodel. Accordingly, the following section discusses the theory behind order reduction and example methods that are generally used.

The final section of this chapter discusses passivity enforcement schemes generally available in the literature. This is because many of the reduced order macromodels lose passivity after the order goes below a certain minimum threshold. To be able to go below that order threshold while maintaining a passive macromodel, then passivity enforcement schemes would be needed.

2.1 System Identification Tools

2.1.1 Least-Squares Approximations

The method of Least-Squares Approximations (LSA) [6] is the one the earliest macromodeling tools utilized to identify the relations between inputs and outputs of an n-port system. It is also one of the simplest in terms of its logic and algorithm. Just like any other regular system, LSA starts off by assuming a system of poles and zeros having unknown coefficients as seen in equation (2.1).

$$Y_{ij}(s) = \frac{a_0 + a_1 s + a_2 s^2 + \ldots + a_n s^n}{b_0 + b_1 s + b_2 s^2 + \ldots + b_n s^n} \tag{2.1}$$

where $s \in (j\omega_1,\ j\omega_2,\ \ldots,\ j\omega_{f-1},\ j\omega_f)$, f is the total number of frequency points for analysis and n is the order of the denominator and numerator polynomials. By multiplying the right and left hand side of equation (2.1) by the poles polynomial, we get a system of $Ax = b$ in terms of the polynomial coefficients. Based on the analysis presented in [6], if n is even and $Y_{ij} = Y_r + jY_i$, the result is seen in equation (2.2) as follows:

$$\begin{aligned} &a_0 + a_1 s + a_2 s^2 + \ldots + a_n s^n \\ &\quad = Y_r b_0 + jY_i s b_1 + Y_r b_2 s^2 + \ldots + jY_i b_{n-1} s^{n-1} + Y_r s^n \end{aligned} \tag{2.2}$$

$$\begin{bmatrix} \omega_1 & \omega_1^3 & \omega_1^5 & \dots & \omega_1^{n-1} & -Y_{1i} & Y_{1i}\omega_1^2 & -Y_{1i}\omega_1^4 & \dots & (-1)^{n/2}Y_{1i}\omega_1^{n-2} \\ \omega_2 & \omega_2^3 & \omega_2^5 & \dots & \omega_2^{n-1} & -Y_{2i} & Y_{2i}\omega_2^2 & -Y_{2i}\omega_2^4 & \dots & (-1)^{n/2}Y_{2i}\omega_2^{n-2} \\ \vdots & \vdots & \vdots & \dots & \vdots & \vdots & \vdots & \vdots & \vdots & \vdots \\ \vdots & \vdots & \vdots & \dots & \vdots & \vdots & \vdots & \vdots & \vdots & \vdots \\ \vdots & \vdots & \vdots & \dots & \vdots & \vdots & \vdots & \vdots & \vdots & \vdots \\ \omega_f & \omega_f^3 & \omega_f^5 & \dots & \omega_f^{n-1} & -Y_{fi} & Y_{fi}\omega_f^2 & -Y_{fi}\omega_f^4 & \dots & (-1)^{n/2}Y_{fi}\omega_f^{n-2} \end{bmatrix} \cdot \begin{bmatrix} a_1 \\ -a_3 \\ a_5 \\ \vdots \\ (-1)^{n/2+1}a_{n-1} \\ b_0 \\ b_2 \\ b_4 \\ \vdots \\ b_{n-2} \end{bmatrix} \tag{2.3}$$

$$= \begin{bmatrix} (-1)^{n/2}Y_{1i}\omega_1^n \\ (-1)^{n/2}Y_{2i}\omega_2^n \\ \vdots \\ \vdots \\ \vdots \\ (-1)^{n/2}Y_{fi}\omega_f^n \end{bmatrix}$$

This system described in equation (2.3) is an $Ax = b$ system where the solution results in the unknown coefficients. The following step is to to do a partial fraction expansion of equation (2.1) with the now known coefficients. However, the system could have unstable right-hand plane poles, which should be eliminated. This results in m poles where $m < n$. Accordingly, the system is portrayed as follows in equation

(2.4):

$$Y_{ij}(s) = k_\infty + \sum_{a=1}^{m} \frac{k_a}{s - p_a} \tag{2.4}$$

where k_i are the residues and p_a are the stable poles (left-hand plane). Further and deeper analysis of LA can be found in [6].

Comments on Least-Square Approximations. The method of LSA has a general advantage of being relatively simple and straightforward. However, with this simplicity comes major drawbacks of it being only good for low-order and narrow frequency-band systems due to its ill conditioning [12].

2.1.2 Vector Fitting

Vector Fitting [9, 10, 5, 26] is one the macromodeling tools utilized commercially nowadays since it has straightforward mathematics, and for most applications, it is accurate enough. As aforementioned, the data is provided in the frequency-domain, hence it could be represented in a pole-zero representation as shown in equation (2.5), where a_i are the zeros and b_i are the poles.

$$f(s) = \frac{a_0 + a_1 s + a_2 s^2 + \ldots + a_N s^N}{b_0 + b_1 s + b_2 s^2 + \ldots + b_N s^N} \tag{2.5}$$

In order to avoid the ill-conditioning issue that was seen in LSA in subsection 2.1.1, direct multiplication by the denominator is avoided. Instead, the system is converted into a pole-residue format for easier application with vector fitting. Equation (2.6) shows the pole-residue format where c_i are the residues and a_i are the poles,

both either real or conjugate pairs, while d and h are real. The conversion from the pole-zero format to the pole-residue format can be done by using the mathematical rules for partial fractions. The reason why the pole-residue format works better for vector fitting is because it produces solutions that are better scaled and conditioned, while being capable of solving systems of higher order [9].

$$f(s) = \sum_{n=1}^{N} \frac{c_n}{s - a_n} + d + sh \tag{2.6}$$

Solving equation (2.6) would require estimating all the coefficients so that $f(s)$ can be estimated over the required range of frequencies required. The equation in its current form is *nonlinear*. Vector Fitting hence divides the problem into a series of 2 sequential steps solving the equations *linearly* given known poles, as follows:

Step 1: Pole Calculation. The first step is to specify a set of starting poles $\bar{a}_n$ and multiplying $f(s)$ by an unknown function $\sigma(s)$, giving the augmented problem as follows in equation (2.7):

$$\begin{bmatrix} \sigma(s)f(s) \\ \sigma(s) \end{bmatrix} = \begin{bmatrix} \sum_{n=1}^{N} \frac{c_n}{s-\bar{a}_n} + d + sh \\ \sum_{n=1}^{N} \frac{\tilde{c}_n}{s-\bar{a}_n} + 1 \end{bmatrix} \tag{2.7}$$

The advantage of using the $\sigma(s)$ function is that at high frequencies the function converges to unity. This hence leads to the following equation which can be written either as equation (2.8a) or as equation (2.8b).

$$\left(\sum_{n=1}^{N}\frac{c_n}{s-a_n}+d+sh\right)\approx\left(\sum_{n=1}^{N}\frac{\tilde{c}_n}{s-\bar{a}_n}+1\right)f(s) \tag{2.8a}$$

$$(\sigma f)_{fit}(s)=\sigma_{fit}(s)f(s) \tag{2.8b}$$

Accordingly, the system at hand can now be solved as an over-determined linear system of $Ax=b$ by taking several frequency points given its unknowns c_i, d, h and $\tilde{c}_i$. Hence a rational function approximation of $f(s)$ can now be readily obtained since both $(\sigma f)_{fit}(s)$ and $\sigma_{fit}(s)$ are known, as shown in equation (2.9a), making $f(s)$ easily calculated as shown in equation (2.9b).

$$(\sigma f)_{fit}(s)=h\frac{\prod_{n=1}^{N+1}(s-z_n)}{\prod_{n=1}^{N}(s-\bar{a}_n)} \quad , \quad \sigma_{fit}(s)=\frac{\prod_{n=1}^{N}(s-\tilde{z}_n)}{\prod_{n=1}^{N}(s-\bar{a}_n)} \tag{2.9a}$$

$$f(s)=\frac{(\sigma f)_{fit}(s)}{\sigma_{fit}(s)}=h\frac{\prod_{n=1}^{N+1}(s-z_n)}{\prod_{n=1}^{N}(s-\tilde{z}_n)} \tag{2.9b}$$

Consequently, we can see from equation (2.9b) that the expression for $f(s)$ is independent of the assumed starting poles $\bar{a}_i$, while the poles of $f(s)$ are the zeros of $\sigma_{fit}(s)$ as shown in [9].

Step 2: Residue Calculation. The residues for $f(S)$ can be calculated directly from equation (2.9b), but for increased accuracy the zeros of $\sigma(s)$ are plugged

into the original equation (2.6) as new poles for the system a_n resulting in another over-determined system $Ax = b$ to be solved for the unknowns c_i, d and h as shown in [9].

Comments on Vector Fitting. Vector fitting results in better conditioning when compared to Least-Squares Approximation. This results in more accurate results generally. However, Vector Fitting holds a major drawback of having difficulties with systems with a large number of poles and large number of ports [12]. This is a major limitation for the method and hence methods such as Loewner Matrix, seen in subsection 2.1.3 were devised to solve that problem.

2.1.3 Loewner Matrix

Loewner Matrix (LM) [25, 19, 12, 17], like all the other system identification methods, is targeted at converting the frequency-domain measured data, such as Y or S-parameters, into a a time-domain macromodel. A Y-Parameters represenation is seen in equation (2.10) where s_k is the complex frequency, $\mathbf{Y}(s_k)$ are the Y-parameters at frequency s_k, and $k = 1, 2, \ldots, n$, with n being the number of data points. Equation (2.10) also shows that the admittance Y-paramaters relate the voltage $V(s_k)$ to the current $I(s_k)$ in the frequency domain.

$$\begin{aligned} &\{s_k, \mathbf{Y}(s_k)\} \\ I(s_k) =& \mathbf{Y}(s_k) V(s_k) \end{aligned} \tag{2.10}$$

On the other hand, the S-parameters representation can be seen in equation (2.11) where all Y-parameters notations stand except that $\mathbf{S}(s_k)$ are the S-parameters at frequency s_k along with $a(s_k)$ and $b(s_k)$ being the incident and reflected power waves

respectively.

$$\begin{aligned} &\{s_k, \mathbf{S}(s_k)\} \\ b(s_k) =& \mathbf{S}(s_k) a(s_k) \end{aligned} \tag{2.11}$$

The incident and reflected power waves $a(s_k)$ and $b(s_k)$, seen in the S-parameters representation, can be converted into a voltage/current representation using the relationships seen in equation (2.12), where z_0 is the normalized impedance, conventionally 50Ω. Figure (2–1) also demonstrates a graphical representation of the incident and reflected waves on an arbitrary N-line system.

$$\begin{aligned} a(s_k) &= \frac{1}{2}\left(\frac{v(s_k)}{\sqrt{z_0}} + i(s_k)\sqrt{z_0}\right) \\ b(s_k) &= \frac{1}{2}\left(\frac{v(s_k)}{\sqrt{z_0}} - i(s_k)\sqrt{z_0}\right) \end{aligned} \tag{2.12}$$

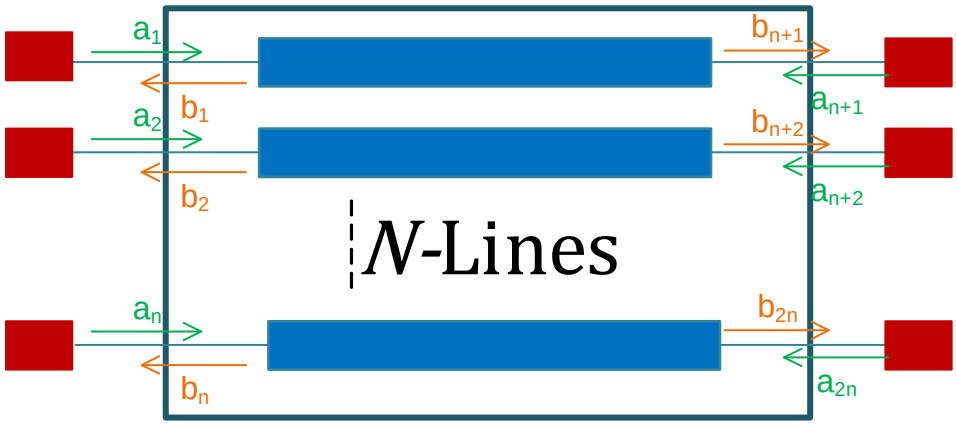

Figure 2–1: N-Line S-Parameter System with Incident and Reflected Power Waves

Accordingly, the macromodel can be represented as a Linear Time-Invariant (LTI) system in Descriptor State-Space (DSS) system representation with p inputs

and outputs. The DSS representation in shown in 2.13 as follows:

$$\begin{aligned} \mathbf{E}\dot{\mathbf{x}}(t) &= \mathbf{A}\mathbf{x}(t) + \mathbf{B}\mathbf{u}(t), \\ \mathbf{y}(t) &= \mathbf{C}\mathbf{x}(t) + \mathbf{D}\mathbf{u}(t) \end{aligned} \tag{2.13}$$

where, $\mathbf{u}(t) \in \mathbb{R}^p$ and $\mathbf{y}(t) \in \mathbb{R}^p$ are the input and output vectors, respectively. For Y-parameters they become the voltage and current vectors, while for S-parameters they become the incident and reflected power waves. $\mathbf{E}, \mathbf{A} \in \mathbb{R}^{m\times m}$, $\mathbf{B} \in \mathbb{R}^{m\times p}$, $\mathbf{C} \in \mathbb{R}^{p\times m}$ and $\mathbf{D} \in \mathbb{R}^{p\times p}$ represent the DSS where m is the order of the system. $\mathbf{E}$ may be singular [4] and the matrix pencil $(\mathbf{A}, \mathbf{E})$ is always regular. Furthermore, the eigenvalues of the matrix pencil $(\mathbf{A}, \mathbf{E})$ are the poles of the system. The order m is determined from the singular value plot in regular LM method [17].

This transfer function for the system $H(s)$ can hence be computed as a division of the output $y(t)$ by the input $u(t)$ as follows in equation (2.14):

$$H(s) = \mathbf{C}(s\mathbf{E} - \mathbf{A})^{-1}\mathbf{B} + \mathbf{D} \tag{2.14}$$

Consequently, the first step of the LM algorithm is appending the frequency domain data with the complex conjugates at the negative frequencies, which would result in $2n$ data points, which is double the original number. This data is then divided into 2 sets, referred to as the left and right data sets, as shown in equation (2.15), where $k = 1, 2, \ldots, 2n$,$i = 1, 2, \ldots, n$, $j = 1, 2, \ldots, n$, and s_k,λ_i and μ_j are complex frequencies:

$$\{s_k, \mathbf{Y}(s_k\} \rightarrow \{\lambda_i, \mathbf{Y}(\lambda_i)\}, \{\mu_j, \mathbf{Y}(\mu_j)\} \tag{2.15}$$

This data splitting can be done in several ways, with the most commonly used ones are the Vector Format Tangential Interpolation (VFTI) [25, 19] and the Matrix Format Tangential Interpolation (MFTI) [32]. Both tracks are presented briefly in this review.

VFTI Data Splitting [25, 19]. VFTI will dedicate the right data set λ for the first half of the frequency points along with their complex conjugates, while the left data set μ would contain the remainder of the data. Equations (2.16a) and (2.16b) show the right and left data sets respectively, where $i = 1, 2, \ldots, \frac{n}{2}$ and $\bar{()}$ is the complex conjugate of the subject.

$$\begin{aligned} \lambda_{2i-1} &= s_i \\ \lambda_{2i} &= \bar{s}_i \end{aligned} \tag{2.16a}$$

$$\begin{aligned} \mu_{2i-1} &= s_{\frac{n}{2}+1} \\ \mu_{21} &= \bar{s}_{\frac{n}{2}+i} \end{aligned} \tag{2.16b}$$

MFTI Data Splitting [32]. MFTI on the other hand aseembles in the right set the odd frequency samples along with their complex conjugates, while the even ones are added to the left set. Equations (2.17a) and (2.17b) show the right and left sets respectively where $i = 1, 2, \ldots, \frac{n}{2}$.

$$\begin{aligned} \lambda_{2i-1} &= s_{2i-1} \\ \lambda_{2i} &= \bar{s}_{2i-1} \end{aligned} \tag{2.17a}$$

$$\begin{aligned} \mu_{2i-1} &= s_{2i} \\ \mu_{21} &= \bar{s}_{2i} \end{aligned} \tag{2.17b}$$

After choosing either VFTI or MFTI for the splitting methodology, the next step is to compute the Loewner Matrix $\mathbb{L}$ and the Shifted Loewner Matrix $\sigma\mathbb{L}$ along with 2 other matrices $\mathbb{F}$ and $\mathbb{W}$ on a block-by-block perspective. Equation (2.18) shows the construction of $\mathbb{L}$ and $\sigma\mathbb{L}$ where $j = 1, 2, \ldots, n$ and $i = 1, 2, \ldots, n$.

$$[\mathbb{L}_{j,i}] = \frac{\mathbf{\Phi}_j \mathbf{R}_i - \mathbf{L}_j \mathbf{\Omega}_i}{\mu_j - \lambda_i} \qquad [\sigma\mathbb{L}_{j,i}] = \frac{\mu_j \mathbf{\Phi}_j \mathbf{R}_i - \lambda_i \mathbf{L}_j \mathbf{\Omega}_i}{\mu_j - \lambda_i} \tag{2.18}$$

Where $\mathbf{\Phi}_j$ and $\mathbf{\Omega}_i$ are defined as follows in equation (2.19), given that $\mathbf{R}_i \in \mathbb{C}^{p \times t_i}$ and $\mathbf{L}_j \in \mathbb{C}^{t_i \times p}$ are the tangential direction matrices for the right and left data sets respectively:

$$\begin{aligned} \mathbf{L}_j \mathbf{Y}(\mu_j) &= \mathbf{\Phi}_j \\ \mathbf{Y}(\lambda_i) \mathbf{R}_i &= \mathbf{\Omega}_i \end{aligned} \tag{2.19}$$

The matrices $\mathbb{F}$ and $\mathbb{W}$ are hence constructed as follows:

$$\begin{aligned} \mathbb{F} &= \begin{bmatrix} \mathbf{\Phi}_1^T \ldots \mathbf{\Phi}_j^T \ldots \mathbf{\Phi}_n^T \end{bmatrix}^T \\ \mathbb{W} &= \begin{bmatrix} \mathbf{\Omega}_1 \ldots \mathbf{\Omega}_i \ldots \mathbf{\Omega}_n \end{bmatrix} \end{aligned} \tag{2.20}$$

Since the computation of $\mathbf{R}_i$ and $\mathbf{L}_j$ is dependent on the tangential interpolation method used, the following paragraphs show the computation of $\mathbf{R}_i$ and $\mathbf{L}_j$ for VFTI and MFTI.

VFTI Tangential Directions Computation [25, 19]. Since VFTI is vector based, this makes the value of $t_i = 1$. Hence $\mathbf{R}_i$ and $\mathbf{L}_j$ are computed as follows:

$$\begin{aligned} \mathbf{R}_{2i-1} &= \mathbf{R}_{2i} = \mathbf{I}_c \\ \mathbf{L}_{2i-1} &= \mathbf{L}_{2i} = (\mathbf{I}_c)^T \end{aligned} \tag{2.21}$$

where $i = 1, 2, \ldots, \frac{n}{2}$ and $\mathbf{I}_c \in \mathbb{R}^{p \times 1}$ is the cth column of the identity matrix of dimension $p \times p$. If $i \texttt{ mod } p = 0$, then $c = p$, otherwise $c = i \texttt{ mod } p$. This can be summarized as $\mathbf{R}_i = \mathbf{L}_i^T$, $\mathbf{L}_j = \mathbf{R}_j^T$ and vice versa.

MFTI Tangential Directions Computation [32]. Since MFTI is matrix based, this sets the value of $t_i = p$ since the matrices are of dimension $p \times p$. This makes the computation of $\mathbf{R}_i$ and $\mathbf{L}_j$ as follows:

$$\begin{aligned} \mathbf{R}_{2i-1} &= \mathbf{R}_{2i} = \mathbf{I} \\ \mathbf{L}_{2i-1} &= \mathbf{L}_{2i} = \mathbf{I} \end{aligned} \tag{2.22}$$

where $i = 1, 2, \ldots, \frac{n}{2}$ and $\mathbf{I} \in \mathbb{R}^{p \times p}$ is an identity matrix.

The Loewner Matrices hence formulated in equations (2.18) and (2.19) are complex and need to be converted to a real ones in order to obtain a real macromodel. This is done by the similarity transformation as follows [19]:

$$\begin{aligned} \mathbb{L}_r &= \mathbb{G}^* \mathbb{L} \mathbb{G}, \quad \sigma \mathbb{L}_r = \mathbb{G}^* \sigma \mathbb{L} \mathbb{G} \\ \mathbb{F}_r &= \mathbb{G}^* \mathbb{F}, \qquad\quad \mathbb{W}_r = \mathbb{W} \mathbb{G} \end{aligned} \tag{2.23}$$

where $\mathbb{G} \in \mathbb{C}^{n \times n}$ is a block-diagonal matrix. Each one of the blocks of $\mathbb{G}$ is hence as follows:

$$g = \frac{1}{\sqrt{2}} \begin{bmatrix} \mathbf{I}_r & -j\mathbf{I}_r \\ \mathbf{I}_r & +j\mathbf{I}_r \end{bmatrix} \tag{2.24}$$

where $\mathbf{I}_r \in \mathbb{R}^{t_i \times t_i}$ is an identity matrix. Since for VFTI $t_i = 1$, hence $\mathbf{I}_r$ will be replaced by a 1, while for MFTI $t_i = p$, so it will remain a matrix.

The next step would be to extract the time-domain macromodel. This can be done by extracting the regular part of the matrix pencil $(x\mathbb{L}_r - \sigma\mathbb{L}_r)$ [25]. One method for extracting the regular part could be done by Singular Value Decomposition (SVD) [25, 19], as follows:

$$x\mathbb{L}_r - \sigma\mathbb{L}_r = \mathbf{\Lambda}\mathbf{\Sigma}\mathbf{\Psi}^* \tag{2.25}$$

where $x \in \{\lambda_i\} \cup \{\mu_j\}$, $\lambda_i, \mu_j \notin eig(\sigma\mathbb{L}_r, \mathbb{L}_r)$, $\mathbf{\Sigma}$ is a diagonal matrix containing the singular values, $\mathbf{\Lambda}$ and $\mathbf{\Psi}$ are the orthonormal matrices and $()^*$ denotes the complex conjugate transpose. Any chosen value of x, $\forall x \in \{\lambda_i\} \cup \{\mu_j\}$, will result in the same SVD, except for when x is one of the eigenvalues [19].

If enough data points were utilized, the matrix pencil $(x\mathbb{L}_r - \sigma\mathbb{L}_r)$ would generally not be full-rank. The regular part of the system if hence extracted by taking the first m columns of $\mathbf{\Lambda}$ and $\mathbf{\Psi}$ to form the orthonormal basis as follows:

$$\begin{aligned} \mathbf{\Lambda}_R &= [\mathbf{\Lambda}_1 \mathbf{\Lambda}_2 \dots \mathbf{\Lambda}_i \dots \mathbf{\Lambda}_m] \\ \mathbf{\Psi}_R &= [\mathbf{\Psi}_1 \mathbf{\Psi}_2 \dots \mathbf{\Psi}_i \dots \mathbf{\Psi}_m] \end{aligned} \tag{2.26}$$

where $\mathbf{\Lambda}_i$ and $\mathbf{\Psi}_i$ are the ith column of $\mathbf{\Lambda}$ and $\mathbf{\Psi}$ respectively and m is the order of the system. The choice and selection of m is a topic that is to be discussed later on in the Order Reduction section of the work.

Accordingly, the time-domain macromodel can now be extracted as follows:

$$\begin{aligned}
\mathbf{E} &= -\mathbf{\Lambda}_R^* \mathbb{L}_r \mathbf{\Psi}_R \\
\mathbf{A} &= -\mathbf{\Lambda}_R^* \sigma \mathbb{L}_r \mathbf{\Psi}_R \\
\mathbf{B} &= \mathbf{\Lambda}_R^* \mathbb{F}_r \\
\mathbf{C} &= \mathbb{W}_r \mathbf{\Psi}_R \\
\mathbf{D} &= 0
\end{aligned} \tag{2.27}$$

Comments on Loewner Matrix Method. Evidently, Loewner Matrix method requires more complex computations compared to Vector Fitting. However, it has the significant advantage of being capable of handling larger and higher order systems more efficiently. This leads to Loewner Matrix method being the chosen system identification method for the work done in this thesis.

2.2 Passivity and Passivity Enforcement

Passivity is one of the critical characteristics of any given system, along with stability and causality. A physical system is denoted as a passive system if and only if it is unable to generate energy on its own [31]. In order to represent this condition mathematically, an n-port network network representation is done for admittance and scattering representations, or as commonly known as Y and S-parameters. For

the Y-parameters case, the condition for a system to be labeled passive is as follows:

$$\int_{-\infty}^{t} v^T(\tau) i(\tau) d\tau \geq 0 \tag{2.28}$$

where the equation applies for all given time t and for all admissible port voltages $v(t)$ and currents $i(t)$. S-parameters on the other hand, which are represented in incident and reflected power waves instead, $a(t)$ and $b(t)$ respectively, which makes the condition for passivity as follows:

$$\int_{-\infty}^{t} \Big[a^T(\tau) a(\tau) - b^T(\tau) b(\tau) \Big] d\tau \geq 0 \tag{2.29}$$

The above conditions, mentioned in equations (2.28) and (2.29), are applicable for both lumped and distributed systems. The equations represent the cumulative net energy absorbed by the system from $-\infty$ to the instant t. A system would hence be passive if such energy is to be positive at any given time t. This is only satisfied if the following 2 conditions apply [31]:

1. More energy is absorbed by the system than generated
2. Potential energy generation occurs after energy absorption

It is worth noting that, according to [35, 36], all passive systems are causal.

The main problem with a non-passive system is that, even if it is stable, when connected to terminations that could potentially be both stable and passive, could result in an overall unstable system. *i.e.* Even if a non-passive system is stable on its own, the overall system when connected to terminations could be unstable. Additionally, passive models are physically consistent. This leads to the need for

passivity enforcement algorithms, which force a non-passive system to become passive without changing much of its intrinsic features. Stability and causality of the system can be easily enforced while fitting the model itself, hence only passivity enforcement deserves special attention [22].

Passivity Enforcement mechanisms generally present a trade-off between the optimality of the produced passive model and the computational cost to generate it. An optimal model is one that is passive in the entire frequency spectrum of interest yet maintains the same behavior of the original non-passive model [22]. Accordingly, based on [23], we can see that Passivity Enforcement schemes can be officially divided into optimal and sub-optimal methods. Optimal methods are capable of providing a single passive model that is closest to the original model in some norm within a given parameterization form, such as methods based on Positive or Bounded Real Lemma Passivity constraints. Methods such as those presented in [29, 21] optimize system poles and residues simultaneously in one single step while methods such as those presented in [3, 24, 2] optimize the poles and residues separately in two different steps. Optimal methods are guaranteed through their convex formulation, which results in high computational demands for both processing and memory.

Sub-optimal methods, on the other hand, are based on approximate linearization of the passivity constraints. This includes methods based on Hamiltonian Matrix Pencil Perturbation and Residue or State-Space Perturbation via Localized constraints at specific frequencies [7, 27, 8, 11, 28]. Such methods are much faster and demand less computational memory, however, they are only approximate since they are iterative methods that demand certain convergence thresholds.

For this thesis, the sub-optimal method of Hamiltonian Matrix Pencil Perturbation is utilized for perturbing the models into passive ones. Since the great strength of Loewner Matrix method, which is the system identification tool used in this thesis, is dealing with high order and large number of ports, a huge model in terms of order or port number can hence be used. Accordingly, even the reduced order model, despite smaller than the original one, could also be too big. With optimal passivity enforcement methods the computational expenditure will be too high. Accordingly, a sub-optimal method is used and its accuracy is good enough, since passivity violation driven out of the order reduction of a Loewner Matrix based model is limited in both frequency spread and extent of violation.

CHAPTER 3
Thesis Contribution

This chapter presents the main thesis contribution, which is centered around system identification of frequency domain S-parameter data using the Loewner Matrix method discussed in 2.1.3, through that order reduction is also achieved, which is discussed in this chapter. This is then followed by Passivity checking and Enforcement algorithm of Hamiltonian Matrix Pencil Perturbation. This is then finalized by an algorithm that converts the macromodel into a spice netlist for universality of the algorithm and convert it into a practical model that can be utilized wherever needed.

3.1 Loewner Matrix

Loewner Matrix is the method utilized in the work done in this thesis for system identification of the frequency domain scattering parameters (S-parameters). The method takes the data as input for the frequency spectrum of interest and produces as output the matrices $\{\mathbf{E}, \mathbf{A}, \mathbf{B}, \mathbf{C}, \mathbf{D}\}$. Details of the macromodeling process and all its mathematics and references are mentioned earlier in subsection 2.1.3.

3.2 Passivity Checking

Choosing the order of the macromodel resulting from the Loewner Matrix method is a process that involves choosing the extent of passivity that can be tolerated by the passivity enforcement algorithm [18]. The reasoning behind this is that there is a certain threshold of order reduction, when reducing the order below which the

system starts to become non-passive by nature. Going further below that threshold induces more extensive passivity violations. According to [18], there is also a maximum passivity violation extent that the Hamiltonian Matrix Pencil Perturbation methodology can handle. Hence, before discussing the order selection process, a method for checking the passivity condition and passivity extent of the macromodel needs to be realized, which is the primary aim of this section.

Equations (2.13) and (2.14) from subsection 2.1.3 describe the Descriptor State Space System and the transfer function resulting from that, respectively. These are the eventual outputs of the Loewner Matrix method, but in the case of scattering S-parameters, the inputs and outputs become the incident and reflected power waves. According to [34] and [33], the DSS can be re-written in Weierstrass Canonical form as follows:

$$\mathbf{E} = W \begin{bmatrix} I_{m_f} & 0 \\ 0 & N \end{bmatrix} T, \qquad \mathbf{A} = W \begin{bmatrix} J & 0 \\ 0 & I_{m_\infty} \end{bmatrix} T \tag{3.1}$$

where W and T are $m \times m$ non-singular matrices, with m being the same m of the Loewner Matrix order. I_j is an identity matrix of dimension j and $m_f + m_\infty = m$. N is a nilpotent matrix of index μ meaning that $N^{\mu-1} \neq 0$ and $N^\mu = 0$, where μ is called the index of the DSS. Accordingly, using the Weierstrass Canonical form, the transfer function in equation (2.14) can be rewritten as follows:

$$H(s) = \underbrace{\mathbf{C}_p(sI_{m_f} - J)^{-1}\mathbf{B}_p + M_0}_{H_p(s)} + \underbrace{\sum_{i=1}^{\mu-1} s^i M_i}_{H_\infty(s)} \tag{3.2}$$

where $M_0 = \mathbf{D} - \mathbf{C}_\infty \mathbf{B}_\infty$, $M_i = -\mathbf{C}_\infty N^i \mathbf{B}_\infty$, $\begin{bmatrix} \mathbf{B}_p \\ \mathbf{B}_\infty \end{bmatrix} = W^{-1}\mathbf{B}$, $\begin{bmatrix} \mathbf{C}_p & \mathbf{C}_\infty \end{bmatrix} = \mathbf{C}T^{-1}$, $H_p(s)$ is called the proper part of the transfer function, while $H_\infty(s)$ is the improper part.

Accordingly, the right and left spectral projector matrices, P_r and P_l respectively, project onto the right and left deflating sub-spaces associated with the finite eigenvalues of the $(\mathbf{A}, \mathbf{E})$ matrix pencil as defined as follows (elaborate details of their calculation is found in [37]):

$$P_r = T^{-1} \begin{bmatrix} I_{m_f} & 0 \\ 0 & 0 \end{bmatrix} T \tag{3.3a}$$

$$P_l = W \begin{bmatrix} I_{m_f} & 0 \\ 0 & 0 \end{bmatrix} W^{-1} \tag{3.3b}$$

where by definition $P_r = P_l^T$ as seen in [37]. It is worth noting that if an improper part exists, the proper part can be extracted either by $\mathbf{E}P_r$ or $P_l\mathbf{E}$.

In consequence, the form seen in equation (3.2) can be tested for passivity as seen in [34] if the following conditions are satisfied:

1. The proper part $H_p(s)$ is bounded real, which implies:
   - $H_p(s)$ has no poles with positive real parts
   - $\sup_{\omega \in \mathbb{R}} \left\{ \sigma_{max}\big(H_p(j\omega)\big) \right\} \leq 1$
2. The improper part $H_\infty(s)$ is zero, *i.e.* $M_i = 0$ for $i \geq 1$

where sup is the supremum mathematical function and $\sigma_{max}(\bullet)$ is the maximum singular value of the subject where $\sigma(M)$, the singular value function, is defined as $\sqrt{\text{eigenvalues}}$ of the self-adjoint matrix (M^*M).

However, the problem with the passivity checking algorithm presented earlier is that the calculation of the Weierstrass Canonical Form is computationally expensive. Accordingly, a more computationally efficient method is needed. Since the Hamiltonian Matrix Pencil matrices are to be calculated anyways for the enforcement of passivity, later on to be presented, [38, 1] show a methodology of using those matrices to check the passivity of the model at hand. The following equation (3.4) shows the definition of the matrices $\mathcal{J}$ and $\mathcal{K}$:

$$\begin{aligned} \mathcal{J} &= \begin{bmatrix} \mathbf{A} - \mathbf{B}\mathbf{D}^T S^{-1}\mathbf{C} & -\mathbf{B}R^{-1}\mathbf{B}^T \\ \mathbf{C}^T S^{-1}\mathbf{C} & -\mathbf{A}^T + \mathbf{C}^T\mathbf{D}R^{-1}\mathbf{B}^T \end{bmatrix} \\ \mathcal{K} &= \begin{bmatrix} \mathbf{E} & \\ & \mathbf{E}^T \end{bmatrix} \end{aligned} \tag{3.4}$$

where $S = \mathbf{D}\mathbf{D}^T - I$ and $R = \mathbf{D}^T\mathbf{D} - I$. The matrix $\mathcal{J} \in \mathbb{R}^{2m\times 2m}$ is called a Hamiltonian matrix and it satisfies the following condition:

$$X_0^{-1}\mathcal{J}X_0 = -\mathcal{J}^T \tag{3.5}$$

where $X_0 = \begin{bmatrix} 0 & I_m \\ -I_m & 0 \end{bmatrix}$ satisfies $X_0^T = X_0^{-1} = -X_0$. Given the same definition of X_0, matrix $\mathcal{K} \in \mathbb{R}^{2m\times 2m}$ is called a symplectic matrix since it satisfies the following

condition:

$$X_0^{-1}\mathcal{K}X_0 = \mathcal{K}^T \tag{3.6}$$

Since $\mathcal{J}$ is Hamiltonian and $\mathcal{K}$ is symplectic, therefore the generalized eigenvalues of the matrix pencil $(\mathcal{J}, \mathcal{K})$ are distributed symmetrically on the complex plane with reference to both real and imaginary axis, *i.e.* eigenvalues reflect on both x and y-axes. Figure 3–1 shows a plot of sample generalized eigenvalues of $(\mathcal{J}, \mathcal{K})$. The green are present in all four quadrants since they are complex (having real and imaginary values), while the blue and red ones are only present in pairs since they are purely imaginary and purely real, respectively.

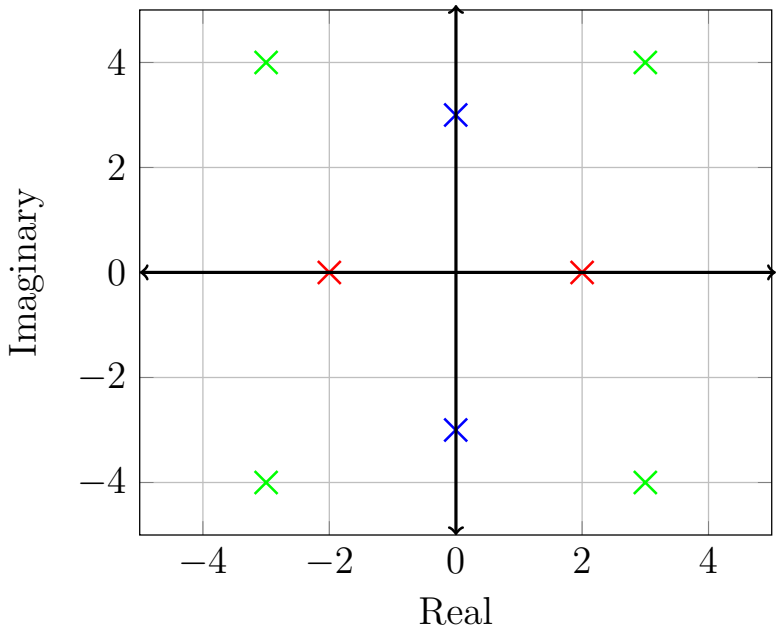

Figure 3–1: Arbitrary Generalized Eigenvalues of $(\mathcal{J}, \mathcal{K})$ Matrix Pencil

Based on [38, 1], the passivity check hence becomes through the same eigenvalues. If there exist eigenvalues of the matrix pencil $(\mathcal{J}, \mathcal{K})$ that are purely imaginary (have no real part), then the system is non-passive; *i.e.* a system is only passive if it has no purely imaginary eigenvalues of the matrix pencil $(\mathcal{J}, \mathcal{K})$.

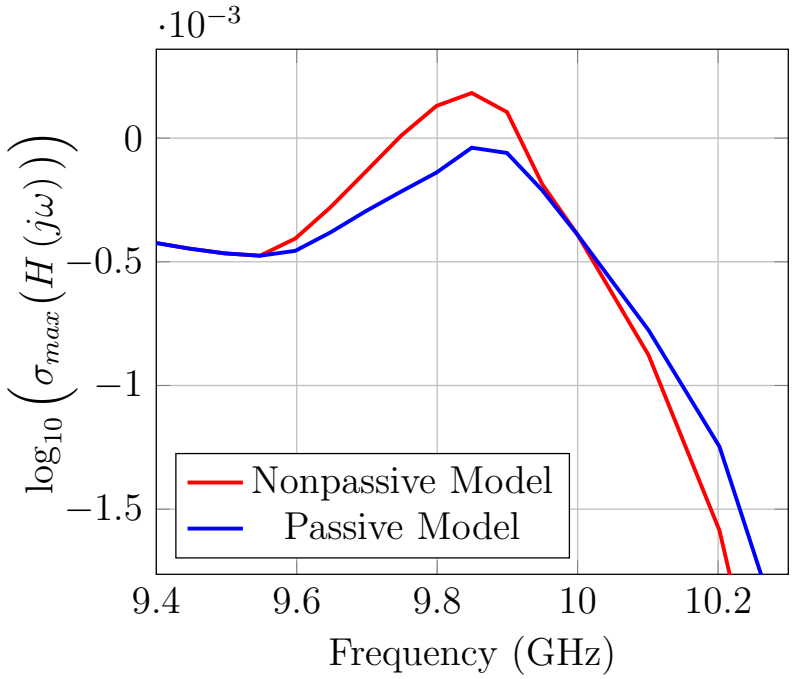

Figure 3–2: Maximum singular values of sample S-parameter matrices with and without a passivity violation

The method of maximum singular values, discussed earlier, can still however be used as an additional check. If the maximum singular value of any frequency point exceeds the value of 1, then the system is non-passive, even if it goes back to below 1 afterwards. Figure 3–2 shows 2 sample systems, with one having a passivity violation between 9.7 and 9.9GHz, and the other one completely passive. The plot is done on

a logarithmic vertical axis, hence the threshold for passivity violation becomes a 0 instead of the original 1.

3.3 Order Reduction

Followed by the method of system identification of Loewner Matrix, it is important to determine the order m to be used to be able to extract the time-domain macromodel. As mentioned before, reducing the order below a certain threshold value would induce a passivity violation. Going further below that value would induce further violation. Given the passivity checking algorithm described in section 3.2, a completely passive order can be found first and then iteratively going below that order in a binary search algorithm till the highest level of passivity to be rectified is reached [18]. For the method of Hamiltonian Matrix Pencil perturbation presented in this thesis, the maximum rectifiable passivity violation is 4 purely imaginary eigenvalues.

3.3.1 Finding Minimal Passive Order

The type of the system being modeled leads to a different response and accordingly a different singular value decomposition pattern. For a lumped system, it is possible for the frequency-domain data to span the full bandwidth of the system, as seen in figure 3–3, which illustrates the forward voltage gain response $S_{2,1}$. This leads to a large drop in the singular values when plotted versus the order as an independent factor, which is shown in figure 3–4, where $\hat{\sigma}_l$ is calculated as follows:

$$\hat{\sigma}_l = \log_{10}\left(\frac{\sigma_l}{\sigma_1}\right) \tag{3.7}$$

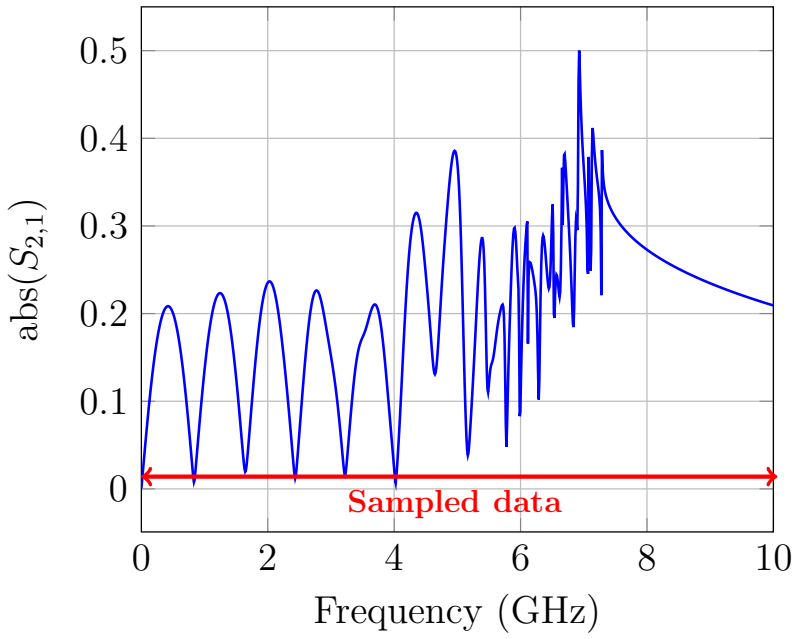

Figure 3–3: Sample S-parameter Data for a Lumped System

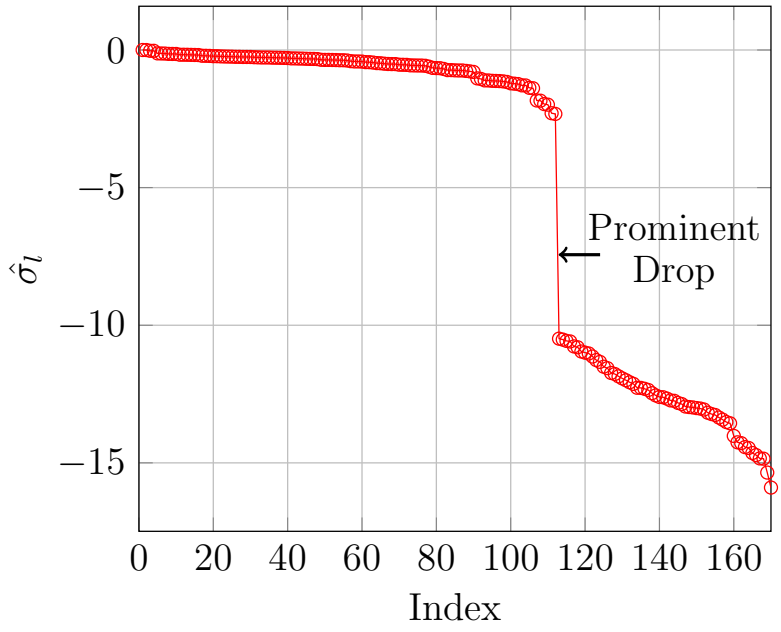

Figure 3–4: Sample Singular Value Decomposition for Lumped System

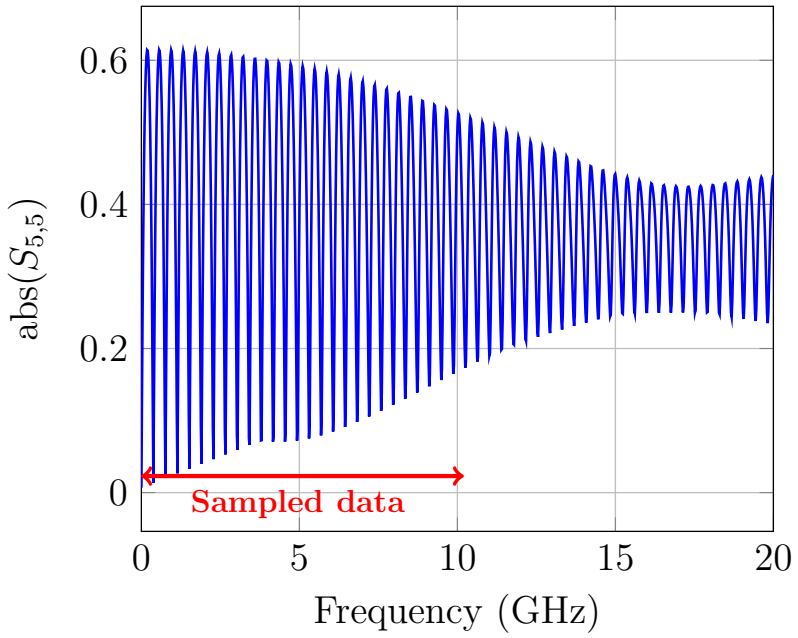

Figure 3–5: Sample S-parameter Data for a Distributed System

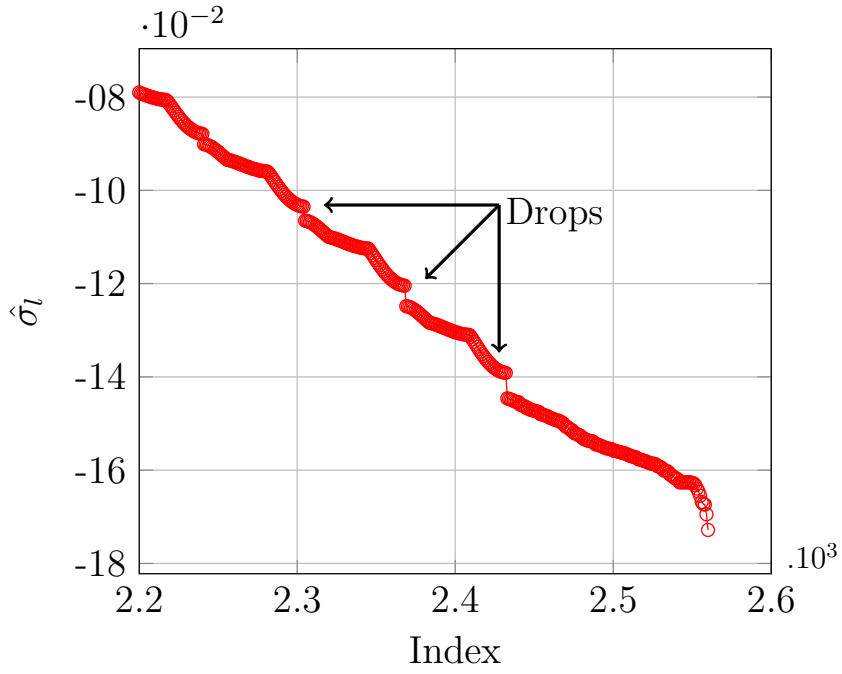

Figure 3–6: Sample Singular Value Decomposition for Distributed System

In this case the order can be easily calculated as seen in [19] based on that significant drop's index. However, for distributed systems, the methodology is not as straightforward as it is for the lumped ones. Figure 3–5 shows that response $S_{5,5}$ keeps ringing in the case of the distributed system, so the sampled data can not reach a decaying steady state value for it *i.e.* it is impossible to span the full bandwidth.

Accordingly, the singular values plot will have no prominent drops similar to the one shown in the lumped system plot. In fact, theoretically, the distributed system is supposed to have an infinite number of poles. However, there are still a few small drops in the singular values of the distributed system as shown in figure 3–6. Such drops are to be used as a basis for a searching algorithm to find the smallest completely passive order to be used as the m_{start} for the order reduction process [16, 14].

The algorithm's first step is calculating the drops among the singular values as follows:

$$\delta_l = \hat{\sigma}_{l+1} - \hat{\sigma}_l; \qquad 1 \leq l \leq pN - 1 \tag{3.8}$$

where δ is the value of the drop, p is the number of ports of the system, N is the number of frequency samples taken for the system resulting in a product pN representing the size of the Loewner Matrix. The drops are then sorted descendingly in a manner as follows:

$$\delta_{i,1} > \delta_{i,2} > \ldots > \delta_{i,x} > \ldots > \delta_{i,pN-1} \tag{3.9}$$

where i, x is the index of the x^{th} largest drop.

Consequently, the order is then chosen starting the largest drop first and the model is extracted. The model is then tested out for passivity using the method explained in section 3.2. If the model turns out to be non-passive, then the next drop is chosen instead, and the same procedure is repeated till a passive macromodel is found and its order is taken to be m_{start}. It is noteworthy that when sufficiently enough data points N are taken and the system is free from noise, typically the largest drop leads to a passive system and hence the previously mentioned algorithm to find m_{start} converges in one iteration [15, 13]. In the presence of noise, such as discretization noise from the full wave simulation, or if the N is just sufficiently large enough, then 2-3 iterations would be needed. If the system takes 5 passivity checking iterations then N needs to be much larger to be able to extract a passive system. Algorithm 1 shows a pseudo-code for the methodology used to find $\{\mathbf{E}, \mathbf{A}, \mathbf{B}, \mathbf{C}\}_{start}$, the macromodel extracted at order m_{start}

Algorithm 1 Determining the order, m_{start} preserving passivity

$k \leftarrow 1$;
$cnvrg \leftarrow 0$;
repeat
  $m \leftarrow ik$;
  Macromodel $\{\mathbf{E}, \mathbf{A}, \mathbf{B}, \mathbf{C}\}$ is extracted as equation (2.27);
  Check for stability and passivity;
  if Macromodel stable and passive **then**
    $m_{start} \leftarrow m$;
    $\{\mathbf{E}, \mathbf{A}, \mathbf{B}, \mathbf{C}\}_{start} \leftarrow \{\mathbf{E}, \mathbf{A}, \mathbf{B}, \mathbf{C}\}$;
    $cnvrg \leftarrow 1$;
  else
    $k \leftarrow k + 1$;
  end if
until $(cnvrg = 1)$ *or* $(k \geq 5)$

3.3.2 Reducing Order Further till Maximum Rectifiable Passivity Violation

Given a passive reduced order m_{start}, it is now desirable to reduce the order even further, to get more benefits out of order reduction. However, from this point onward, further order reduction results in passivity violation. This subsection describes the algorithm used to find the the maximum correctable passivity violation, 4 generalized purely imaginary eigenvalues of the $(\mathcal{J}, \mathcal{K})$ matrix pencil, in the system at hand.

The order finding methodology is very similar to the root finding algorithm of bisection method. We start off with an upper order bound m_{upper} equal to m_{start} and a lower bound m_{lower} equal to $\frac{m_{start}}{2}$. The average value of the 2 bounds is taken as the testing order m_{test}, if its passivity violation is more than tolerable then the order is increased. On the other hand if the passivity violation is still tolerable, then the order is reduced even further. This process is repeated till the required number of purely imaginary eigenvalues is found, which is 4 [18]. This methodology is explained in a pseudo-code form in Algorithm 2 to reach a final order m_f and a macromodel $\{\mathbf{E}, \mathbf{A}, \mathbf{B}, \mathbf{C}\}_f$.

3.3.3 Determining Purely Imaginary Eigenvalues of $(\mathcal{J}, \mathcal{K})$

This subsection describes the two methodologies that could be used to determine whether some of the eigenvalues of the $(\mathcal{J}, \mathcal{K})$ matrix pencil, the Hamiltonian and symplectic matrices, are purely imaginary or not. According to [34], rounding error results in a real part to exist in eigenvalues even if they were supposed to be purely imaginary. This calls for the need of a methodology to determine whether an eigenvalue is to be considered purely imaginary or not.

Algorithm 2 Determining the order, m_f for maximum rectifiable passivity violation

$cnvrg \leftarrow 0$;
$m_{upper} \leftarrow m_{start}$
repeat
  $m_{lower} \leftarrow round\left(\frac{m_{upper}}{2}\right)$;
  $m_{test} \leftarrow round\left(\frac{m_{upper}+m_{lower}}{2}\right)$
  Macromodel $\{\mathbf{E}, \mathbf{A}, \mathbf{B}, \mathbf{C}\}_{test}$ is extracted as equation (2.27);
  Check for passivity;
  if Macromodel passivity < 4 purely imaginary eigenvalues **then**
    $m_{upper} \leftarrow m_{test}$;
  else if Macromodel passivity > 4 purely imaginary eigenvalues **then**
    $m_{upper} \leftarrow round\left(\frac{6}{5} * m_{upper}\right)$;
  else
    $m_f \leftarrow m_{test}$
    $cnvrg \leftarrow 1$
    $\{\mathbf{E}, \mathbf{A}, \mathbf{B}, \mathbf{C}\}_f \leftarrow \{\mathbf{E}, \mathbf{A}, \mathbf{B}, \mathbf{C}\}_{test}$;
  end if
until $(cnvrg = 1)$

Methodology 1. The first method, which is relatively straight forward is shown in [7]. This method involves deciding on a certain value δ as a threshold value. If the real value of the eigenvalue is less than delta *i.e.* $\mathbb{R}\{\lambda\} < \delta$, then the eigenvalue λ is to be considered purely imaginary, and vice versa.

The problem with this methodology, however, is that some eigenvalues could inherently have a real part, but it happens to be small value and not a rounding error. In such case, this methodology would consider such eigenvalue as a purely imaginary one mistakenly, causing the system to be assumed to be non-passive when it could actually be passive. Additionally, if the value of δ is chosen to be smaller than it should be, a purely imaginary eigenvalue having a real part larger than the

value of δ due to rounding errors could be ignored, and hence its passivity violation will not be put into consideration.

Figure 3–7 shows a plot with sample eigenvalues and an arbitrary $\delta \approx 0.12$. The green eigenvalues are ones which are not purely imaginary, but are considered so mistankenly, while the red pair could be purely imaginary yet are not inspected. This shows that this methodology is good to give a general idea about whether eigenvalues are purely imaginary or not, but not good enough to give a detailed perspective.

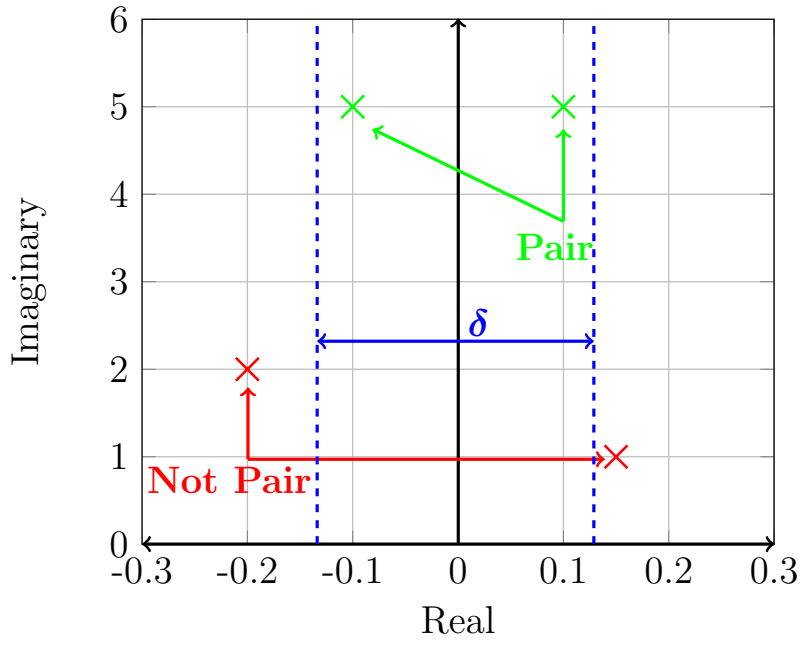

Figure 3–7: Sample Pairing and Non-Pairing Eigenvalues of $(\mathcal{J}, \mathcal{K})$ Matrix Pencil

Methodology 2. This method is more robust than the other method mentioned earlier. It is a variation of the procedure presented in [34]. This technique relies on the fact that all the eigenvalues of the $(\mathcal{J}, \mathcal{K})$ matrix pencil come in pairs

of mirror images across all 4 quadrants, but the reflection across the imaginary axis is of most interest in this case. The method starts by taking picking a value for δ that is big enough, such as 0.2, to include all the eigenvalues that could be purely imaginary but having a large error in the real value. This narrows down the number of eigenvalues that are to be inspected and tested. The eigenvalues left within such a bound are to be tested if they have a pairing mirror image across the imaginary axis. If there exists a pair then the eigenvalues are not to be considered purely imaginary and vice versa.

The first step in realizing whether a two eigenvalues are a pair or not is to inspect the imaginary value first. If the absolute value of the percentage difference between their imaginary values is less than 1%, then they lie on the same vertical level. The following equation describes the test on two eigenvalues λ_i and λ_j:

$$\left| \frac{\mathbb{R}\{\lambda_i\} - \mathbb{R}\{\lambda_j\}}{\mathbb{R}\{\lambda_i\}} \right| < 1\% \tag{3.10}$$

If the eigenvalues are found to be on the same vertical level, then they need to be tested for the horizontal value through testing their real parts. If the eigenvalues λ_i and λ_j are a pair, then their real parts will have opposite sign, hence the absolute value of the real parts' sum should be zero ideally. However, for error compensation the method used takes the percentage change of such difference to be less than 1% to consider the eigenvalues a pair. This is shown in the following equation:

$$\left| \frac{\mathbb{I}\{\lambda_i\} + \mathbb{I}\{\lambda_j\}}{\mathbb{I}\{\lambda_i\}} \right| < 1\% \tag{3.11}$$

Consequently, we see that if the conditions in equations (3.10) and (3.11) are satisfied, then the eigenvalues λ_i and λ_j are a pair. If the condition is not satisfied, then the eigenvalues within the region of δ should be looped through and tested with respect to λ_i till a par is found. If all eigenvalues have been looped and none are found to pair, λ_i is hence to be considered as a purely imaginary eigenvalue. Figure 3–7 also shows how the green eigenvalues are a pair, while the red ones are not a pair, making the former a regular complex eigenvalue (not purely imaginary) while the latter could be purely imaginary, depending on the chosen value for δ.

3.4 Passivity Enforcement

After the order m_f has been chosen, which introduces slight passivity but has the advantage of being a lower order than the previously mentioned m_{start}, passivity enforcement would now be needed to eliminate that violation. The methodology used in this work is based on the Hamiltonian Matrix Pencil Perturbation, or sometimes referred to as Generalized Hamiltonian Method (GHM) theorem, shown in [34].

This method is one of the sub-optimal methods of passivity enforcement, but it ideal for this application. Since passivity violation is limited to only 4 eigenvalues of the $(\mathcal{J}, \mathcal{K})$ matrix pencil, the iterative perspective will not be a problem in this case because only very few iterations would be needed to rectify the violation. This also results in having very accurate results, even if they are approximate, because the region of non-passivity is limited. This makes the method accurate in terms of comparing the responses of the original non-passive model to the passive one, and

also relatively low computational complexity with respect to number of iterations, making it ideal for the applications presented in this work.

Accordingly this part is divided into three main subsections; Model Conversion, Impulse Checking and Proper Part Perturbation, the three main steps of enforcing passivity. Model Conversion changes the model into an alternative form that fits into the GHM theorem, if the given model does not fit. Impulse Checking checks for the availability of an improper part in the system's transfer function. Proper Part Perturbation is the main process of changing aspects about the macromodel iteratively till a passive model is realized.

3.4.1 Model Conversion

The model will need conversion to an alternative form if one or both of the following conditions are present:

$$0 \in eig\left(\mathbf{D} + \mathbf{D}^T\right) \tag{3.12a}$$

$$1 \in \sigma(\mathbf{D}) \tag{3.12b}$$

where $eig(\bullet)$ are the eigenvalues of the subject and $\sigma(\bullet)$ are the singular values of the subject, as defined earlier in section 3.2. Hence, an alternative model for the matrices $(\mathbf{E}, \mathbf{A}, \mathbf{B}, \mathbf{C}, \mathbf{D})$ to become $(\mathbf{E}_{conv}, \mathbf{A}_{conv}, \mathbf{B}_{conv}, \mathbf{C}_{conv}, \mathbf{D}_{conv})$, where the latter model avoids the conditions in equations (3.12a) and (3.12b). By choosing a value for k satisfying $0 < k < 1$, the following is how the converted macromodels can

be created:

$$\mathbf{E}_{conv} = \begin{bmatrix} \mathbf{E} & 0 \\ 0 & 0 \end{bmatrix} \qquad \mathbf{A}_{conv} = \begin{bmatrix} \mathbf{A} & 0 \\ 0 & I_p \end{bmatrix}$$
$$\mathbf{B}_{conv} = \begin{bmatrix} \mathbf{B} \\ kI_p - \mathbf{D} \end{bmatrix} \qquad \mathbf{C}_{conv} = \begin{bmatrix} \mathbf{C} & I_p \end{bmatrix} \tag{3.13}$$
$$\mathbf{D}_{conv} = kI_p$$

where I_p is an identity matrix of dimension p, the same dimension previously described in subsection 2.1.3. The resulting converted models are identical models in terms of their characteristics and response [38], however they have lost the undesirable conditions mentioned in equations (3.12a) and (3.12b). This can also be guaranteed by checking $I - \mathbf{D}_{conv}\mathbf{D}_{conv}^T = (1-k^2)I$ to be non-singular, which is certain in this case [34]. Computational complexity of the whole model conversion process is very low since it is merely a reassembly process of the matrices into bigger ones. If no model conversion is found to be needed, then the converted matrices would be identical to the original ones *i.e.* $\{\mathbf{E}_{conv}, \mathbf{A}_{conv}, \mathbf{B}_{conv}, \mathbf{C}_{conv}, \mathbf{D}_{conv}\} = \{\mathbf{E}, \mathbf{A}, \mathbf{B}, \mathbf{C}, \mathbf{D}\}$.

3.4.2 Impulse Checking

For passivity violation to be rectified using GHM theorem, the system cannot have an improper part $H_\infty(s)$, as mentioned in section 3.2, which is also referred to as the impulsive response. Hence, the process of impulse checking needs to be done before undergoing the perturbation process to validate its usability. The Weierstrass Canonical form described in section 3.2 can be used to extract the transfer function in the form of the proper and improper part, and check for the availbility or absence of

the impulsive response. However, according to [34], the Weierstrass Canonical form is very computationally expensive and ill-conditioned. Accordingly, this subsection displays an alternative method to be used for the same purpose. The following limit is to be used as a checking algorithm for the impulsive response:

$$\Gamma = \lim_{s \to \infty} s^{-1} H(s) \tag{3.14}$$

where Γ is a limit matrix of dimension $p \times p$ and s^{-1} is a scalar multiplied to the transfer function matrix $H(s)$. Accordingly, the following set of conditions define the interpretation of Γ:

1. If $\Gamma = 0 \rightarrow$ System is impulse free; passivity is rectifiable
2. If $\Gamma = constant \neq 0$ or $\Gamma = \infty \rightarrow$ System has improper part; definitely non-passive

For even further simplification of the impulse checking process, the method could be approximated by picking two large positive numbers s_1 and s_2, governed by the relationship of $S_1 = \gamma s_2$ where $3 < \gamma < 10$. The system can hence be checked for impulsive response as follows:

1. If $\frac{\|H(s_1)\|_2}{\|H(s_2)\|_2} \ll \gamma \rightarrow \gamma = 0 \rightarrow$ Impulse-free
2. If $\frac{\|H(s_1)\|_2}{\|H(s_2)\|_2} = \gamma \rightarrow \gamma = constant \rightarrow$ Definitely non-passive
3. If $\frac{\|H(s_1)\|_2}{\|H(s_2)\|_2} \gg \gamma \rightarrow \gamma = constant \rightarrow$ Definitely non-passive

It is noteworthy that since the discussed systems are all stable, hence all poles are distributed on the left half of the complex plane. Accordingly, choosing a positive value for s, as done here in the choice of s_1 and s_2, will always result in an invertible (non-singular) matrix $(s\mathbf{E}_{conv} - \mathbf{A}_{conv})$. According to [34], this method is numerically

stable and highly efficient. Computational complexity of this process is very low since it only includes plugging in certain values and computing system responses.

3.4.3 Proper Part Perturbation

After model conversion was done, if needed, and the system checked for the absence of the impulsive response, it is now turn for the perturbation process of the proper part from a non-passive to a passive one. According to GHM theorem, a system can be changed from non-passive to passive status if the $(\mathcal{J}, \mathcal{K})$ matrix pencil is perturbed. The $(\mathcal{J}, \mathcal{K})$ matrix pencil is made out of the five different model matrices $\{\mathbf{E}_{conv}, \mathbf{A}_{conv}, \mathbf{B}_{conv}, \mathbf{C}_{conv}, \mathbf{D}_{conv}\}$. We hence have five different options for the perturbation process. Reference [34] shows a summary of why some of those matrices could be modified to enforce passivity, while others cannot, as follows:

- Matrices $\mathbf{E}_{conv}$ and $\mathbf{A}_{conv}$ cannot be modified, since that would jeopardize the system's stability condition. It can also change the key dynamic properties of the system at hand, which would hurt the accuracy of the newly generated model.
- Matrix $\mathbf{D}_{conv}$ cannot be perturbed, because that would result in inaccuracy in the entire frequency band of interest.
- Matrices $\mathbf{B}_{conv}$ and $\mathbf{C}_{conv}$ are suitable for the perturbation process, especially since the transfer function $H(s)$ is linear with respect to $\mathbf{B}_{conv}$ and $\mathbf{C}_{conv}$. Matrix $\mathbf{C}_{conv}$ is chosen arbitrarily over $\mathbf{B}_{conv}$ for the perturbation process.

The next step is to create criterion that can be used to control the error introduced by perturbing the matrix $\mathbf{C}_{conv}$. This methodology is based on the one presented in [34]. Given the impulse response, $h(t)$, the inverse Laplace transform of

the transfer function, the error of the perturbed model can be measured as follows:

$$\Delta = \int_0^\infty \|dh(t)\|_F^2 dt = \int_0^\infty trace\left(dh(t)dh^T(t)\right) dt \tag{3.15}$$

where $trace(M)$ is the sum of all the elements in the diagonal of matrix M. Hence, by defining $dh(t) = d\mathbf{C}_{conv}\mathcal{F}(t)\mathbf{B}_{conv}$ with $\mathcal{F}(t) = T^{-1}\begin{bmatrix} e^{jt} & 0 \\ 0 & 0 \end{bmatrix} W^{-1}$, we can rewrite the error function as follows:

$$\Delta = trace\left(d\mathbf{C}_{conv}\mathcal{G}_{pc}d\mathbf{C}^T\right) \tag{3.16}$$

where $\mathcal{G}_{pc}$ is the proper controllability Gramian defined as follows:

$$\mathcal{G}_{pc} = \int_0^\infty \mathcal{F}(t)\mathbf{B}_{conv}\mathbf{B}_{conv}^T\mathcal{F}^T(t)dt \tag{3.17}$$

However, an easier method can be used to compute the Gramian $\mathcal{G}_{pc}$ would be through solving the generalized Lyapunov equations [30] as follows:

$$\begin{gathered} \mathbf{E}_{conv}\mathcal{G}_{pc}\mathbf{A}_{conv}^T + \mathbf{A}_{conv}\mathcal{G}_{pc}\mathbf{E}_{conv}^T = -P_l\mathbf{B}_{conv}\mathbf{B}_{conv}^T P_r \\ \mathcal{G}_{pc} = P_r\mathcal{G}_{pc} \end{gathered} \tag{3.18}$$

By performing a Cholesky Decomposition on the Gramian $\mathcal{G}_{pc} = L^T L$, a coordinate transformation for $d\mathbf{C}_t$, the small perturbation matrix for the original $\mathbf{C}_{conv}$, can hence be done as follows:

$$d\mathbf{C}_t = d\mathbf{C}_{conv}L^T \tag{3.19}$$

Thus, we can redefine the error function as follows:

$$\Delta = trace\left(d\mathbf{C}_t d\mathbf{C}_t^T\right) = \|d\mathbf{C}_t\|_F^2 = \|vec(d\mathbf{C}_t)\|_2^2 \tag{3.20}$$

where $vec(M)$ is a vector created by stacking all the columns of the matrix M.

Since the the original matrix $\mathbf{C}_{conv}$ would be perturbed by the small matrix $d\mathbf{C}_{conv}$, the Hamiltonian and symplectic matrices $\mathcal{J}$ and $\mathcal{K}$ respectively, would also be perturbed. This can be done by differentiating them with respect to the matrix $\mathbf{C}_{conv}$. Since the symplectic matrix $\mathcal{K}$ is independent of $\mathbf{C}_{conv}$, hence its change matrix (derivative) would be a zero as follows:

$$d\mathcal{K} = \begin{bmatrix} 0 & 0 \\ 0 & 0 \end{bmatrix} \tag{3.21}$$

On the other hand, the Hamiltonian matrix $\mathcal{J}$ is dependent on the matrix $\mathbf{C}_{conv}$ as seen in section 3.2. This hence results in a derivative change matrix as follows:

$$d\mathcal{J} = \begin{bmatrix} -\mathbf{B}\mathbf{D}^T S^{-1} d\mathbf{C} & 0 \\ d\mathbf{C}^T S^{-1}\mathbf{C} + \mathbf{C}^T S^{-1} d\mathbf{C} & d\mathbf{C}^T \mathbf{D} R^{-1} \mathbf{B}^T \end{bmatrix} \tag{3.22}$$

where, as defined before, $S = \mathbf{D}\mathbf{D}^T - I$ and $R = \mathbf{D}^T\mathbf{D} - I$, and both matrices are symmetric. It is also noteworthy that the matrix $d\mathcal{J}$ is also Hamiltonian like the original matrix $\mathcal{J}$.

For every generalized eigenvalue $\lambda \in \mathbb{C}$ of the matrix pencil $(\mathcal{J}, \mathcal{K})$, there exist right and left eigenvectors x and $y \in \mathbb{C}^m$ such that:

$$\begin{aligned} \mathcal{J}x &= \lambda \mathcal{K}x \\ y^*\mathcal{J} &= \lambda y^*\mathcal{K} \end{aligned} \tag{3.23}$$

The generalized eigenvalue λ can therefore be written as a tuple $\langle \alpha, \beta \rangle$, with $\lambda = \frac{\alpha}{\beta}$. Hence, if $\beta = 0$, λ is an infinite eigenvalue. Hence upon perturbing the purely imaginary eigenvalues of the $(\mathcal{J}, \mathcal{K})$ matrix pencil, they change form from λ to λ', which can hence be described as follows:

$$\lambda' = \frac{\alpha'}{\beta} = \frac{\alpha + \Delta\alpha}{\beta} = \lambda + \frac{y^* d\mathcal{J}x}{y^*\mathcal{K}x} \tag{3.24}$$

According to [34], if λ is purely imaginary, then λ' is also purely imaginary. Accordingly, we can design a set $\Lambda = \{\lambda_i\} = \{j\omega_i\}$ for $i = 1, 2, \ldots, q$ for all the q purely imaginary eigenvalues of the matrix pencil $(\mathcal{J}, \mathcal{K})$. This divides the entire frequency band from $0 \to \infty$ into $q + 1$ segments, with all the eigenvalues in the set Λ need to be perturbed, since $\sigma\big(H(j\omega_i)\big) > 1$. Accordingly, in order to perturb ω_i to $\tilde{\omega}_i$, we use the following equation:

$$\begin{aligned} \tilde{\omega}_i &= \omega_i + \epsilon(\omega_{i+1} - \omega_i) \\ 0 &< \epsilon < 0.5 \end{aligned} \tag{3.25}$$

However since the newly calculated $\tilde{\omega}_i$ is relatively arbitrary, this should be treated as a new new input to the system and the passivity checking procedure should be reiterated. This is the iterative part of the passivity enforcement algorithm. Based

on [34], for mild passivity violation, which is the case here, the number of iterations should not exceed five.

The next step is to plug in the perturbed frequency values $\tilde{\omega}_i$'s into the system in order to compute the perturbed matrix $\tilde{\mathbf{C}}_{conv}$ in lieu of the old non-passive $\mathbf{C}_{conv}$. Firstly, the right eigenvector x_i is to be split into two vectors of the same size, becoming $x_i = \begin{bmatrix} x_{i,1} \\ x_{i,2} \end{bmatrix}$. Secondly, it will be denoted that $z_i = S^{-1}\left(\mathbf{C}_{conv}x_{i,1} + \mathbf{D}_{conv}\mathbf{B}_{conv}^{T}x_{i,2}\right)$. Then, based on [34], we can create an equation containing $d\mathbf{C}_t$ as follows:

$$\mathbb{R}\left\{\left(x_{i,1}^{T}L^{-1}\right)\otimes z_i^{*}\right\} \times vec(d\mathbf{C}_t) = (\tilde{\omega}_i - \omega_i)\mathbb{I}\left\{x_{i,2}^{*}\mathbf{E}x_{i,1}\right\} \tag{3.26}$$

where $\otimes$ is the Kronecker product of two subjects. From the previous equation (3.26) we can extract two block matrices m_i and n_i denoting the equation (3.26)'s main subjects, as follows:

$$m_i = \mathbb{R}\left\{\left(x_{i,1}^{T}L^{-1}\right)\otimes z_i^{*}\right\} \tag{3.27a}$$

$$n_i = (\tilde{\omega}_i - \omega_i)\mathbb{I}\left\{x_{i,2}^{*}\mathbf{E}x_{i,1}\right\} \tag{3.27b}$$

In such case, if there exists q eigenvalues to be moved, then the block matrices m_i and n_i can be incorporated into larger matrices and vectors $\mathbf{M}$ and $\mathbf{N}$ as follows:

$$\mathbf{M} = \begin{bmatrix} m_1 \\ m_2 \\ \vdots \\ m_q \end{bmatrix} \in \mathbb{R}^{q \times pm}, \qquad \mathbf{N} = \begin{bmatrix} n_1 \\ n_2 \\ \vdots \\ n_q \end{bmatrix} \in \mathbb{R}^{q \times 1} \tag{3.28}$$

This would results in an equation of the form

$$M \times vec(d\mathbf{C}_t) = N \tag{3.29}$$

which can be used solve for the desired unknown $vec(d\mathbf{C}_t)$ which can then be easily transformed from vector form back to matrix form of $d\mathbf{C}_t$. Equation (3.29) is a standard least-squares problem to be solved, however, the constraint is an underdetermined equation since the number of unknowns pm far exceeds the number of equations q *i.e.* $q \ll pm$. Based on [34], there are two possible ways to solve equation (3.29), which are as follows:

1. Pseudoinverse Method: Solution would be $vec(d\mathbf{C}_t) = \mathbf{M}^T(\mathbf{M}\mathbf{M}^T)^{-1}\mathbf{N}$
2. QR-Factorization Method: Solution would be $vec(d\mathbf{C}_t) = Q_{\mathbf{M}}R_{\mathbf{M}}^{-T}\mathbf{N}$ with $Q_{\mathbf{M}}R_{\mathbf{M}} = \mathbf{M}^T$ is the QR-factorization of $\mathbf{M}^T$

After finding the value of $d\mathbf{C}_t$, the perturbed matrix $\tilde{\mathbf{C}}_{conv}$ can hence be found as follows:

$$\tilde{\mathbf{C}}_{conv} = \mathbf{C}_{conv} + d\mathbf{C}_t L^{-T} \tag{3.30}$$

This would result in a new passive model $\left\{\mathbf{E}_{conv}, \mathbf{A}_{conv}, \mathbf{B}_{conv}, \tilde{\mathbf{C}}_{conv}, \mathbf{D}_{conv}\right\}$ with a reduced order m_{final}.

3.5 SPICE Netlist Generation

The next step is to generate a SPICE netlist of the model described by the matrices $\left\{\mathbf{E}_{conv}, \mathbf{A}_{conv}, \mathbf{B}_{conv}, \tilde{\mathbf{C}}_{conv}, \mathbf{D}_{conv}\right\}$ having a reduced order m_{final}. Since this model is stable and now passive, it can be used for generic modeling along with any other device or terminations, which also are stable and passive, hence producing an overall stable system that does not produce energy on its own. The benefit of the SPICE netlist is its universality, since the netlist would be generic and any other device or terminations can be easily connected to the model at hand, whether those be linear or nonlinear.

There are several ways to generate a netlist from a DSS model, however, [16] presents a methodology of creating a SPICE netlist using the Modified Nodal Analysis (MNA) formulations. The macromodel matrices $\left\{\mathbf{E}_{conv}, \mathbf{A}_{conv}, \mathbf{B}_{conv}, \tilde{\mathbf{C}}_{conv}, \mathbf{D}_{conv}\right\}$ are stamped into the MNA equation and we can hence generate a circuit node for every port. A similar approach, but for Y-parameter data can be seen in [20]. The methodology implies considering the input and output voltages at the ports of the model at hand. However, for S-parameter based systems, the incident and reflected power waves $a(s_k)$ and $b(s_K)$ are what characterize the model, as seen in equation 2.12, which is reiterated in the following equation:

$$\begin{aligned} a(s_k) &= \frac{1}{2}\left(\frac{v(s_k)}{\sqrt{z_0}} + i(s_k)\sqrt{z_0}\right) \\ b(s_k) &= \frac{1}{2}\left(\frac{v(s_k)}{\sqrt{z_0}} - i(s_k)\sqrt{z_0}\right) \end{aligned} \tag{3.31}$$

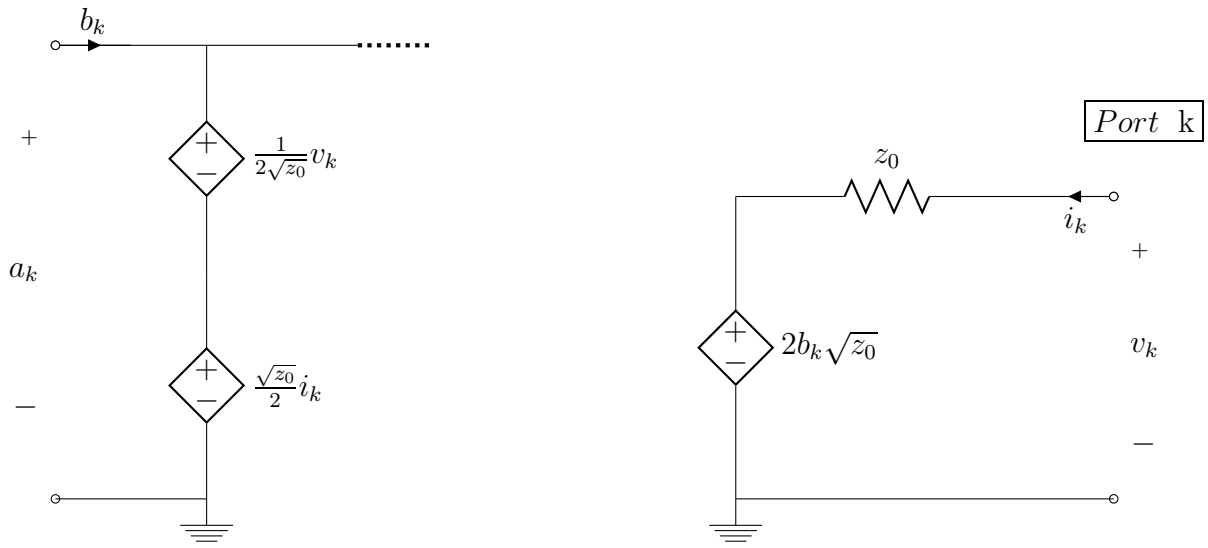

Figure 3–8: Equivalent Voltage-Current Realization of Terminal Power Wave Representations

where z_0 is any arbitrary reference impedance, which could be used as the standard 50Ω. Hence, there needs to be a way of converting such system which is based on power waves to expressions in terms of the voltages and currents. This implies having extra circuitry to the MNA equation at hand which would handle such a conversion. The circuitry used is based on [16] and is seen in voltage-controlled voltage sources as well as current-controlled voltage sources that are seen in figure 3–8.

CHAPTER 4
Implementation Examples

This chapter presents several examples to prove the functionality and evaluate the performance of the previously proposed algorithms. The following examples are all based on 10cm long microstrip lines with varying number of 1mm wide traces. The separation between the traces is 0.2mm. More elaborate details of the generic microstrip line used is shown in figure 4–1.

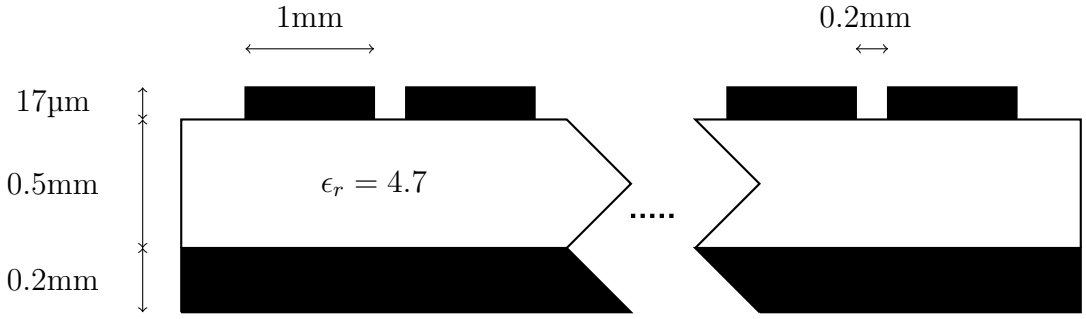

Figure 4–1: Microstrip line structure

The structures at hand are first defined in terms of their Per-Unit Length (PUL) parameter matrices, then the required number of S-parameter data is generated using the matrix exponential stamp. This is then followed by macromodeling using LM, determining the lowest order achieving the maximum rectifiable passivity violation m_{final} and finally enforcing the passivity on the model at hand.

4.1 Example 1: 8-Traces Microstrip Line

The first examples pertain a microstrip line that has 8 traces, also presented in [18], hence has 16 ports. The original system has an order $m = 358$. This order is reduced substantially to an $m_{start} = 275$ and eventually reaching a final reduced non-passive order of $m_{final} = 271$. Passivity is then enforced using the GHM theorem, with an optimal $\epsilon = 0.4$. We see that the passivity enforcement algorithm converges in 2 iterations only, and the time for macromodeling using LM is 1.04 seconds and the time for passivity rectification is 2.75 seconds.

4.1.1 Correctness Validation

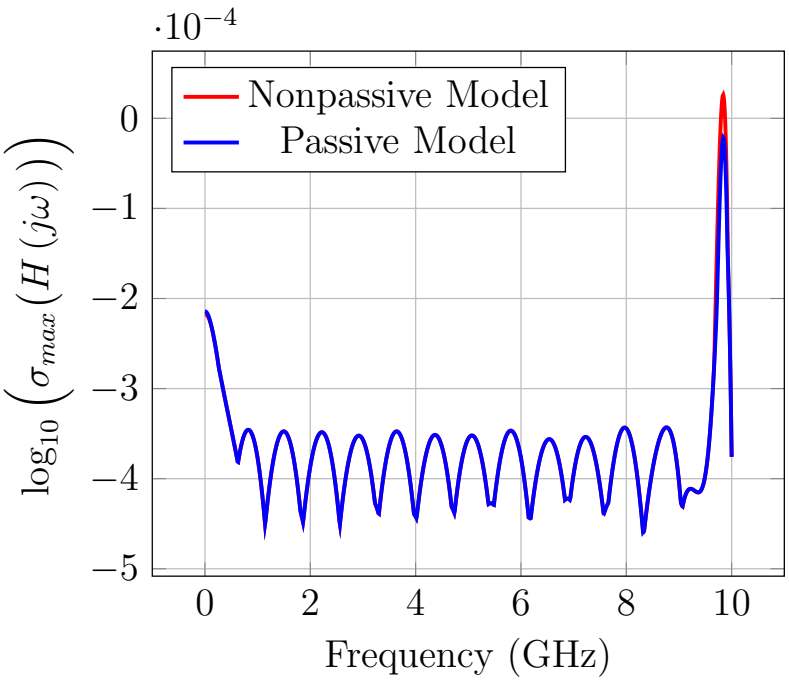

Figure 4–2: Maximum Singular Values of Example 1's S-Parameter Matrices Before and After Passivity Enforcement

Figure 4–2 shows the maximum singular values of the example at hand before and after passivity enforcement. Evidently, the non-passive model has singular values crossing the maximum threshold of 1 (0 on the logarithmic scale in the plot), while the passive model is below that mark. Figure 4–3 shows a magnified version of the same plot with the region of passivity violation shown clearly to be 9.78 → 9.89GHz. The plots also demonstrate that the passivity violation has been corrected efficiently.

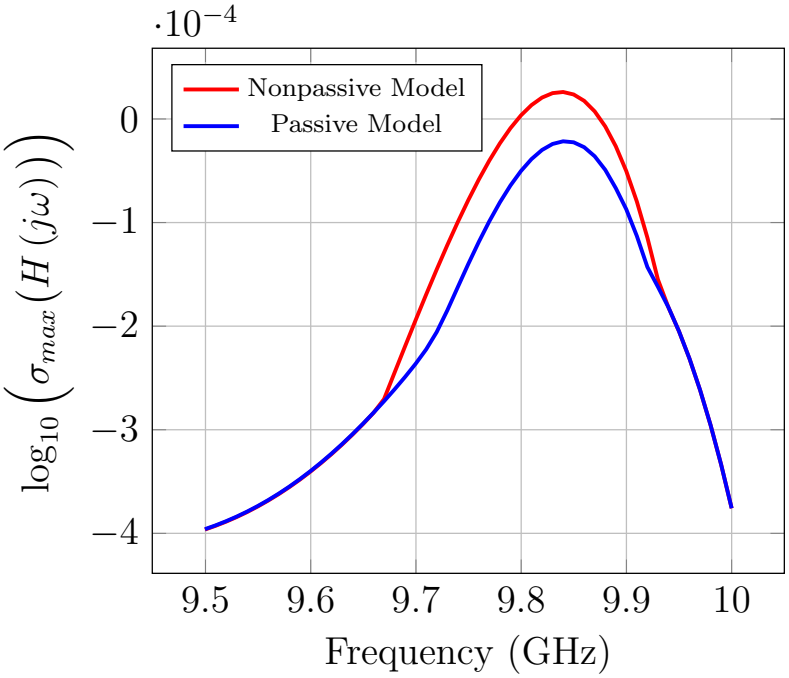

Figure 4–3: Magnified Maximum Singular Values of Example 1's S-Parameter Matrices Before and After Passivity Enforcement

4.1.2 Accuracy Validation

After proving the success of the modeling and passivity enforcement parts, this part discusses the error produced by both process. When computed across 1000 frequency point within the frequency range of interest, it has been found that the

Root Mean Squared (RMS) error as resulting from the macromodeling process is 5.9×10^{-5}, while the overall RMS error after passivity enforcement is 7.5×10^{-5}, both of which are very insignificant numbers, showing that the whole process is accurate to a great extent. This also verifies that the passivity enforcement scheme is both functional and accurate. A plot of the RMS error across the entire frequency range is found in figure 4–4.

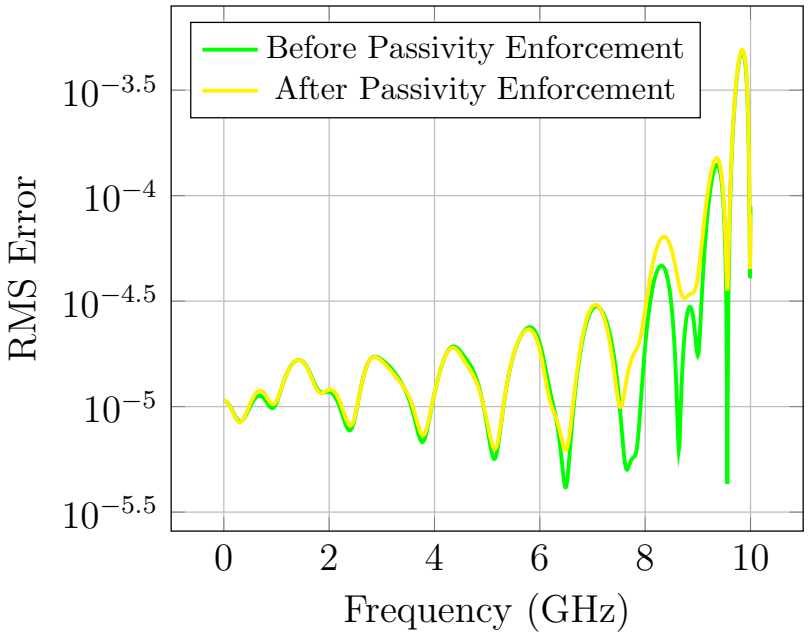

Figure 4–4: RMS Error Across Frequency Spectrum for Example 1

Plots of magnitude and phase of original vs. perturbed models were evaluated for further verification. Figures 4–5 and 4–6 show an aggressor line response at index $(10, 10)$, while figures 4–7 and 4–8 show a victim line response at index $(2, 16)$. The four plots validate correctness and negligible loss of accuracy in perturbation while achieving smaller order m_{final}.

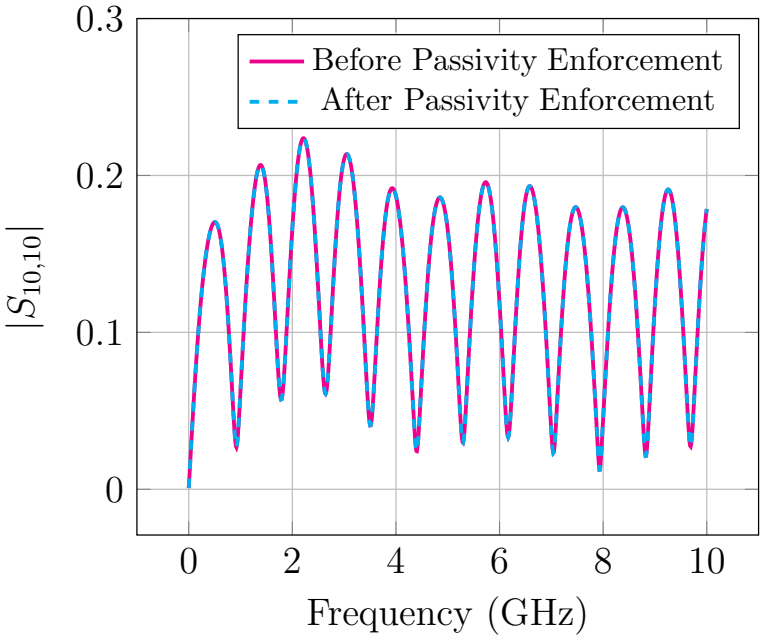

Figure 4–5: Magnitude of Aggressor Line Response at $(10, 10)$ for Example 1

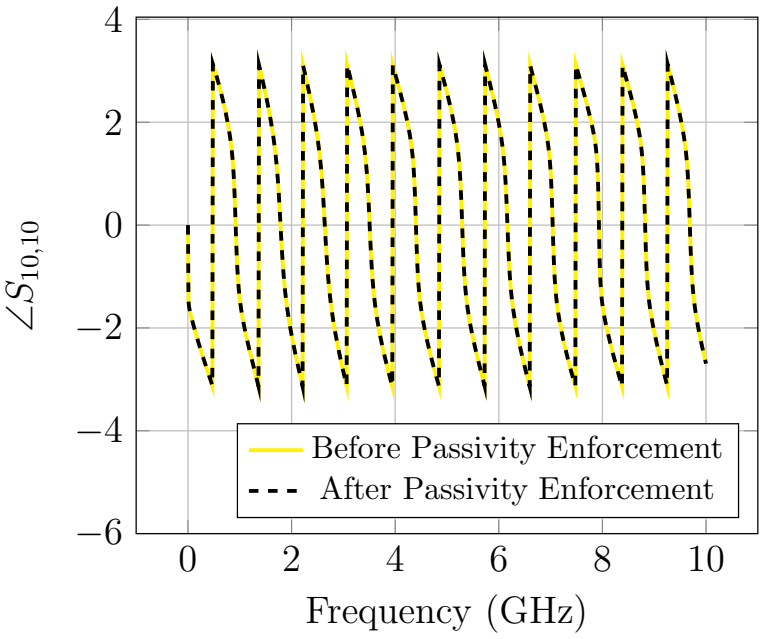

Figure 4–6: Phase of Aggressor Line Response at $(10, 10)$ for Example 1

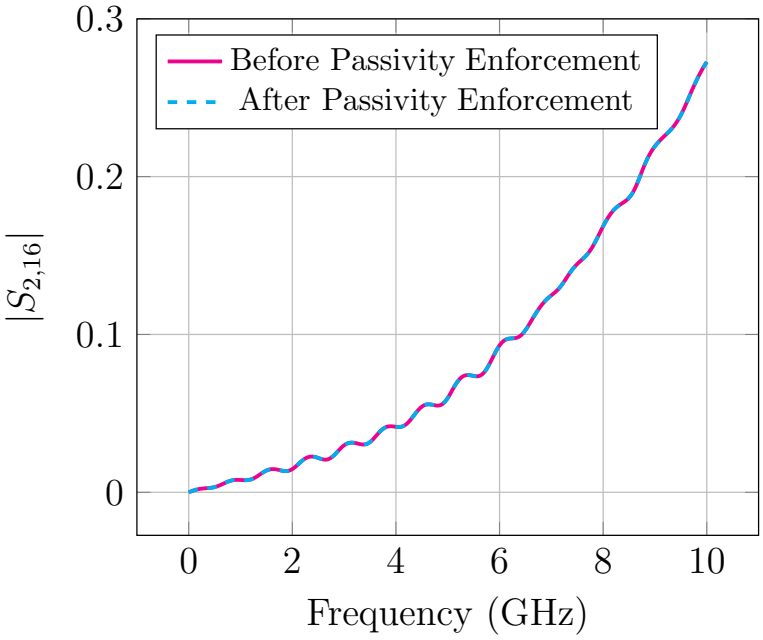

Figure 4–7: Magnitude of Victim Line Response at $(2, 16)$ for Example 1

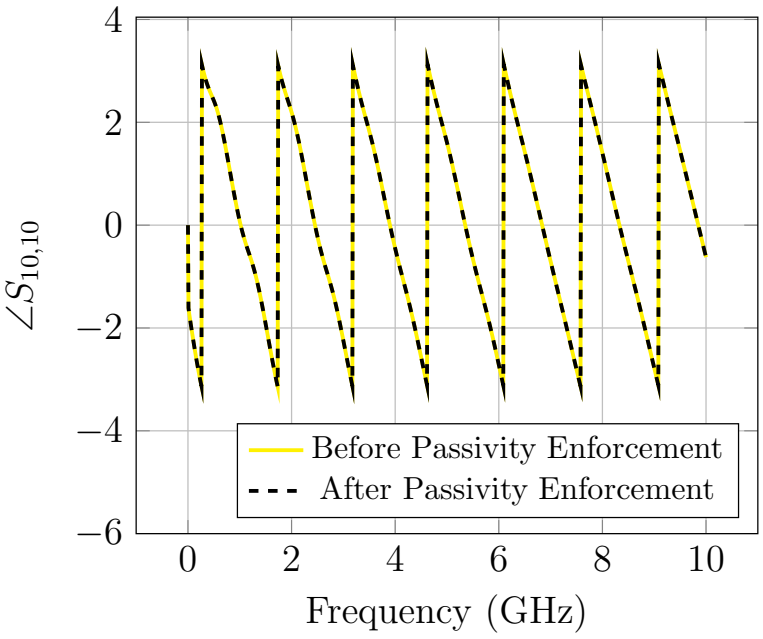

Figure 4–8: Phase of Victim Line Response at $(2, 16)$ for Example 1

4.2 Example 2: 16-Traces Microstrip Line

The second example, also discussed in [18], is larger than the first example with double the number of traces in the microstrip line *i.e.* 16 traces, matching to 32 ports in the system. The original system has an order $m = 725$, which is then reduced to $m_{start} = 544$ and eventually reaching a final reduced non-passive order of $m_{final} = 537$. As with the previous example, passivity enforcement is performed using the GHM theorem, finding an optimal value for $\epsilon = 0.35$. As with the previous example, the system converges in 2 iterations only with a macromodeling time of 3.35 seconds using LM, while the time for the passivity correction is 20.63 seconds. The time taken for the passivity rectification is considerably longer than that taken for the first example, because the passivity violation is more extensive in this example, in addition to the system generally having more eigenvalues for the $(\mathcal{J}, \mathcal{K})$ matrix pencil.

4.2.1 Correctness Validation

Figure 4–9 shows the maximum singular values of for the second example before and after passivity rectification. Evidently, we see that, just like the first example, the original system had passivity violation, illustrated by crossing the 1 boundary in its singular value decomposition. After the passivity rectification, the singular values no longer cross that boundary, proving successful perturbation in the system. Figure 4–10 shows a magnified version of the same plot illustrating the region of passivity violation being within $9.74 \rightarrow 9.92$GHz. Upon Comparing figures 4–3 to 4–10, we see that the extent of the passivity violation (the height of the peak) is way higher for example 1, explaining the increase in computation time.

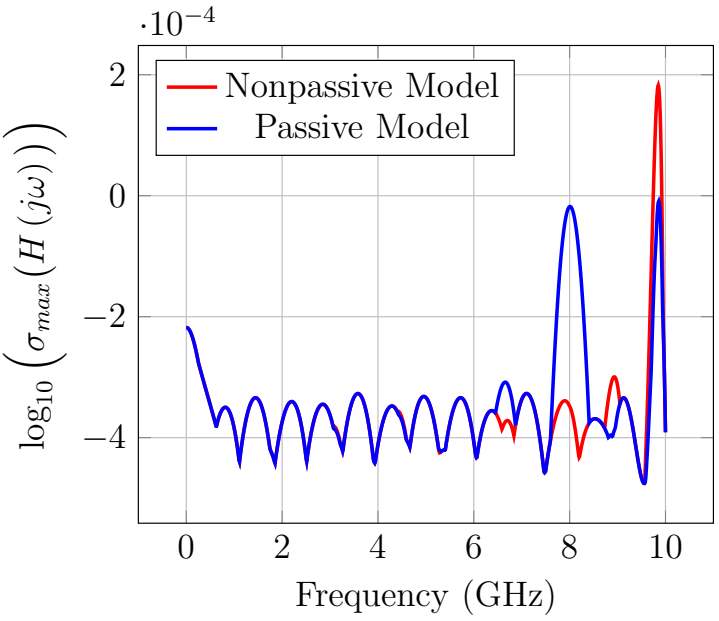

Figure 4–9: Maximum Singular Values of Example 2's S-Parameter Matrices Before and After Passivity Enforcement

4.2.2 Accuracy Validation

Similar to the first example, an error analysis over 1000 frequency points from DC to 10GHz. The results of the error analysis show that macromodeling process results in an overall RMS error of 3.9×10^{-5}, while after passivity perturbation, the overall RMS error increased only to 5.3×10^{-5}. This shows that the process is also accurate, and no significant accuracy is lost in the passivity perturbation process. Figure 4–11 further elaborates on the same conclusions by showing the error trends along the frequency range of interest.

Plots of magnitude and phase of original vs. perturbed models were evaluated for further verification. Figures 4–12 and 4–13 show an aggressor line response at index $(4, 4)$, while figures 4–14 and 4–15 show a victim line response at index $(8, 12)$.

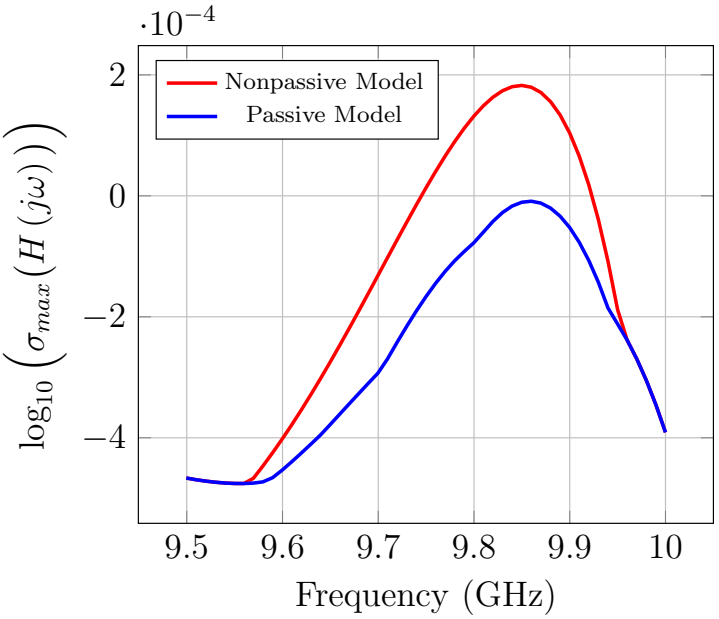

Figure 4–10: Magnified Maximum Singular Values of Example 2's S-Parameter Matrices Before and After Passivity Enforcement

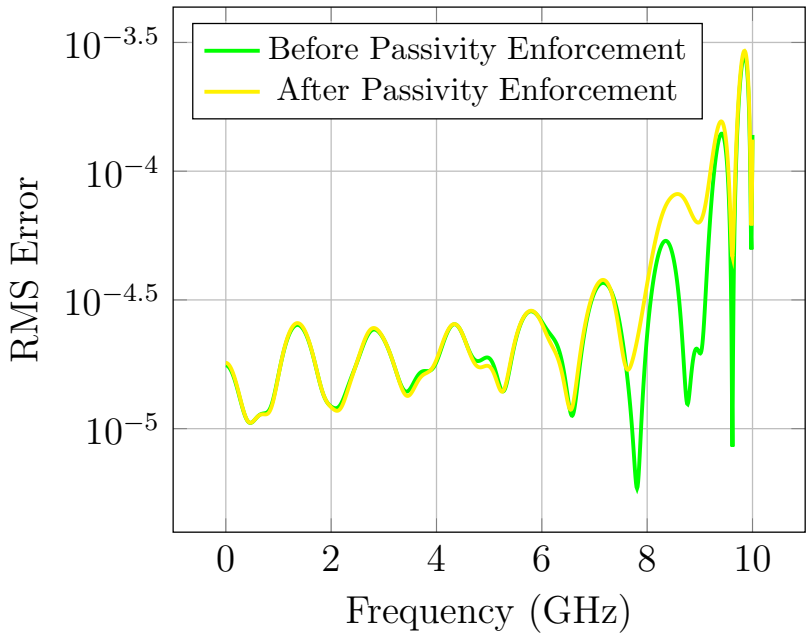

Figure 4–11: RMS Error Across Frequency Spectrum for Example 2

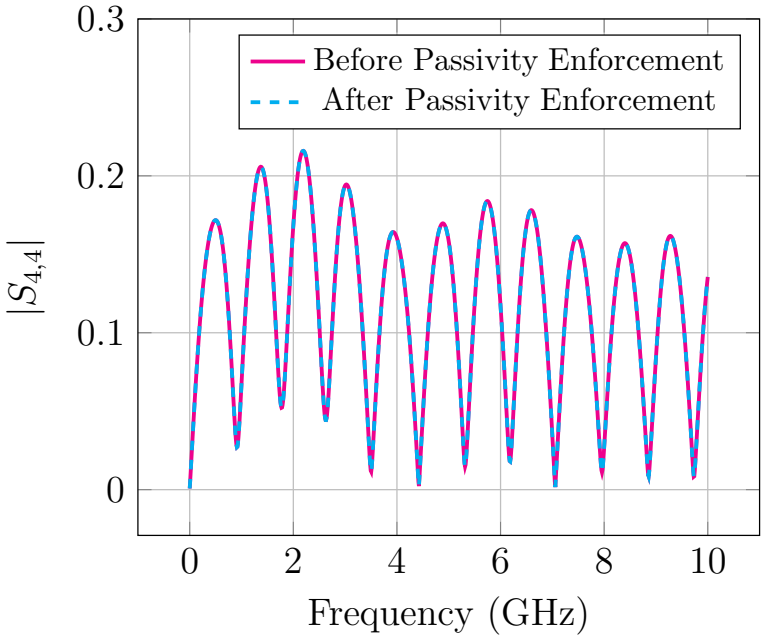

Figure 4–12: Magnitude of Aggressor Line Response at $(4, 4)$ for Example 2

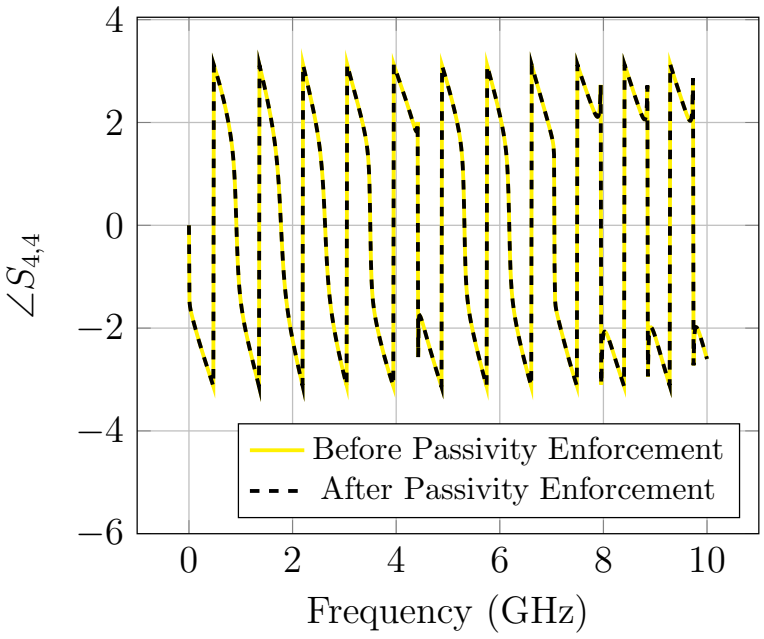

Figure 4–13: Phase of Aggressor Line Response at $(4, 4)$ for Example 2

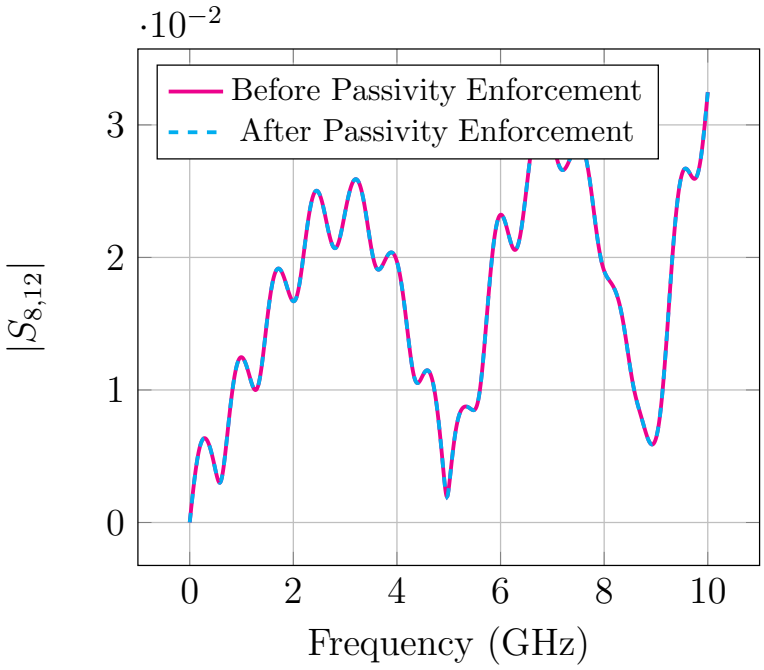

Figure 4–14: Magnitude of Victim Line Response at $(8, 12)$ for Example 2

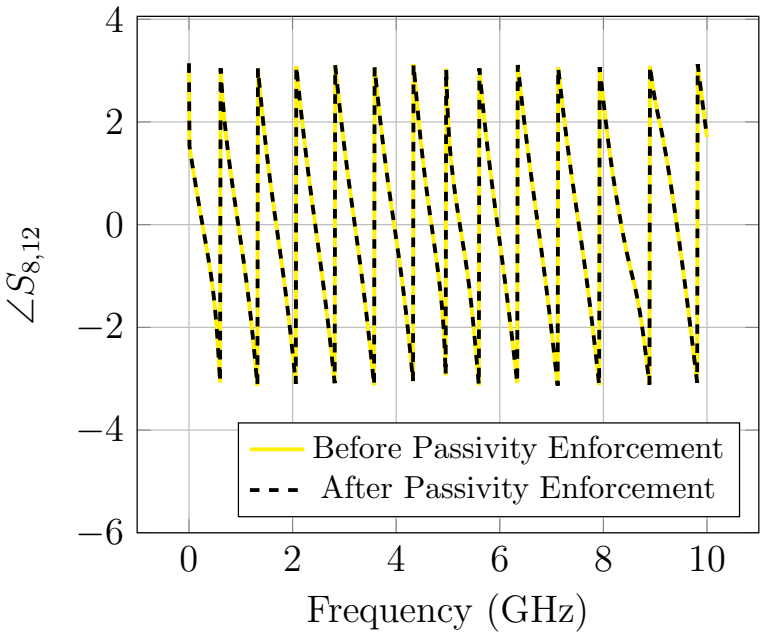

Figure 4–15: Phase of Victim Line Response at $(8, 12)$ for Example 2

CHAPTER 5
Conclusion

To sum up the work presented in this thesis, we see that we can undergo order reduction of system macromodels in a very efficient way. This is done by first utilizing system identification methods, such as Loewner Matrix in this case, choosing a much reduced order that results in mild passivity violation, then correcting that passivity violation using passivity enforcement schemes such as Hamiltonian Matrix Pencil Perturbation. The advantage of following such a scheme is that we can reach a much reduced order than the one that could have been reached by using the standard model order reduction methodologies. This is done at a minor computational cost, as seen in table 5–1, which summarizes the results and parameters from the examples described in chapter 4. The table shows that as the size of the system increases, the computational time for passivity rectification increases, but the number of iterations needed to converge remains the same. Generally, the bulk of the computational expenditure comes from the passivity rectification algorithm, but this is countered by its main advantage of being capable of reaching a much reduced order compared to the original one. The only drawback is that the algorithm is not capable of handling severe passivity violations, or else it would take way too many iterations and computational time, but this can be fixed by changing the passivity enforcement scheme to another one that suits the application at hand.

Table 5–1: Examples Parameters and Characteristics Summary

Parameter		Example 1	Example 2
# of Lines		8	16
# of Ports		16	32
Original Order m		358	725
Final Order m_{final}		271	537
ϵ		0.4	0.35
# of Iterations		2	2
Simulation Time (seconds)	Loewner Matrix	1.04	3.35
	Passivity Enforcement	2.75	20.63
Passivity Violation Spectrum (GHz)		$9.78 \leq f \leq 9.89$	$9.74 \leq f \leq 9.92$

In terms of the accuracy of the methodology being used, the systems yield highly accurate responses compared to the original models at hand. Table 5–2 can be seen as a summary of the overall RMS errors for the examples shown in chapter 4. The table shows that the GHM theorem, while as mentioned before might not be suitable for high passivity violations, is perfectly suitable for mildly non-passive systems, which in this case is limited to 4 eigenvalues of the $(\mathcal{J}, \mathcal{K})$ matrix pencil. The table

Table 5–2: Examples Error Summary

Error	Example 1	Example 2
Before Passivity Enforcement	5.9×10^{-5}	3.9×10^{-5}
After Passivity Enforcement	7.5×10^{-5}	5.3×10^{-5}

shows that the GHM theorem, while as mentioned before might not be suitable for high passivity violations, is perfectly suitable for mildly non-passive systems, which in this case is limited to 4 eigenvalues of the $(\mathcal{J}, \mathcal{K})$ matrix pencil. So the resulting model described by $\left\{\mathbf{E}_{conv}, \mathbf{A}_{conv}, \mathbf{B}_{conv}, \tilde{\mathbf{C}}_{conv}, \mathbf{D}_{conv}\right\}$ can be seen to be a stable,

passive, and much reduced in order than the original system while maintaining highly accurate physical characteristics when compared to each other.

References

[1] P. Benner, V. Sima, and M. Voigt. $\mathcal{L}_\infty$-norm computation for continuous-time descriptor systems using structured matrix pencils. *Automatic Control, IEEE Transactions on*, 57(1):233–238, 2012.

[2] G. C. Calafiore, A. Chinea, and S. Grivet-Talocia. Subgradient Techniques for Passivity Enforcement of Linear Device and Interconnect Macromodels. *IEEE Transactions on Microwave Theory Techniques*, 60:2990–3003, October 2012.

[3] Carlos P Coelho, Joel Phillips, and Luis Miguel Silveira. A convex programming approach for generating guaranteed passive approximations to tabulated frequency-data. *Computer-Aided Design of Integrated Circuits and Systems, IEEE Transactions on*, 23(2):293–301, 2004.

[4] Liyi Dai. Singular control systems, 1989.

[5] D. Deschrijver and T. Dhaene. Passivity-based sample selection and adaptive vector fitting algorithm for pole-residue modeling of sparse frequency-domain data. In *Behavioral Modeling and Simulation Conference, 2004. BMAS 2004. Proceedings of the 2004 IEEE International*, pages 68–73, 2004.

[6] M. Elzinga, K. L. Virga, and J. Prince. Improved global rational approximation macromodeling algorithm for networks characterized by frequency-sampled data. *Microwave Theory and Techniques, IEEE Transactions on*, 48(9):1461–1468, 2000.

[7] S. Grivet-Talocia. Passivity enforcement via perturbation of hamiltonian matrices. *Circuits and Systems I: Regular Papers, IEEE Transactions on*, 51(9):1755–1769, 2004.

[8] S. Grivet-Talocia. An adaptive sampling technique for passivity characterization and enforcement of large interconnect macromodels. *Advanced Packaging, IEEE Transactions on*, 30(2):226–237, 2007.

[9] B. Gustavsen and A. Semlyen. Rational approximation of frequency domain responses by vector fitting. *Power Delivery, IEEE Transactions on*, 14(3):1052–1061, 1999.

[10] B. Gustavsen and A. Semlyen. A robust approach for system identification in the frequency domain. *Power Delivery, IEEE Transactions on*, 19(3):1167–1173, 2004.

[11] B. Gustavsen and A. Semlyen. Fast passivity assessment for -parameter rational models via a half-size test matrix. *Microwave Theory and Techniques, IEEE Transactions on*, 56(12):2701–2708, 2008.

[12] M. Kabir and R. Khazaka. Macromodeling of distributed networks from frequency-domain data using the loewner matrix approach. *Microwave Theory and Techniques, IEEE Transactions on*, 60(12):3927–3938, 2012.

[13] M. Kabir and R. Khazaka. Parametric macromodeling of high-speed modules from frequency-domain data using loewner matrix based method. In *Microwave Symposium Digest (IMS), 2013 IEEE MTT-S International*, pages 1–4, 2013.

[14] M. Kabir and R. Khazaka. Order selection for loewner matrix based macromodels for accurate macromodeling of distributed high-speed modules from limited number of full-wave s-parameter data. In *Signal and Power Integrity (SPI), 2014 IEEE 18th Workshop on*, pages 1–4, 2014.

[15] M. Kabir, R. Khazaka, R. Achar, and M. Nakhla. Loewner-matrix based efficient algorithm for frequency sweep of high-speed modules. In *Electrical Performance of Electronic Packaging and Systems (EPEPS), 2012 IEEE 21st Conference on*, pages 185–188, 2012.

[16] Muhammad Kabir and Roni Khazaka. Mflm: *s*-parameter based macromodeling using matrix format loewner matrix interpolation. Submitted for Review.

[17] Muhammad Kabir and Roni Khazaka. Order selection for loewner matrix based macromodels for accurate macromodeling of distributed high-speed modules from limited number of full-wave S-parameter data. In *IEEE 18th Workshop on Signal and Power Integrity (SPI), 2014*, pages 1–4, May 2014.

[18] Marco Kassis, Muhammad Kabir, and Roni Khazaka. Passive reduced order macromodeling using hamiltonian matrix pencil perturbation. In *International*

Conference on Numerical Electromagnetic and Multiphysics Modeling and Optimization for RF, Microwave and Terahertz Applications NEMO , IEEE MTT-S, 2015.

[19] S. Lefteriu and A. C. Antoulas. A new approach to modeling multiport systems from frequency-domain data. *Computer-Aided Design of Integrated Circuits and Systems, IEEE Transactions on*, 29(1):14–27, 2010.

[20] Z. Liu, M. Kabir, and R. Khazaka. Time-domain spice macromodel of high-speed modules from y-parameter data using loewner matrix approach. In *Proc. International Conference on Analog VLSI Circuits (AVIC)*, pages 90–93, 2013.

[21] Z. Mahmood, B. Bond, T. Moselhy, A. Megretski, and L. Daniel. Passive reduced order modeling of multiport interconnects via semidefinite programming. In *Design, Automation and Test in Europe Conference and Exhibition (DATE), 2010*, pages 622–625, 2010.

[22] Z. Mahmood, S. Grivet-Talocia, A. Chinea, G. C. Calafiore, and L. Daniel. Efficient localization methods for passivity enforcement of linear dynamical models. *Computer-Aided Design of Integrated Circuits and Systems, IEEE Transactions on*, 33(9):1328–1341, 2014.

[23] Zohaib Mahmood, Stefano Grivet-Talocia, Giuseppe C. Calafiore, and Luca Daniel. Optimal passivity enforcement of state-space models via localization methods. In *Electrical Performance of Electronic Packaging, 2014 IEEE*, pages 89–92, 2014.

[24] Zohaib Mahmood, Roberto Suaya, and Luca Daniel. An efficient framework for passive compact dynamical modeling of multiport linear systems. In *Proceedings of the Conference on Design, Automation and Test in Europe*, pages 1203–1208. EDA Consortium, 2012.

[25] A. J. Mayo and A. C. Antoulas. A framework for the solution of the generalized realization problem. *Linear Algebra And Its Applications*, 425(2-3):634–662, 2007.

[26] D. Saraswat, R. Achar, and M. S. Nakhla. A fast algorithm and practical considerations for passive macromodeling of measured/simulated data. *Advanced Packaging, IEEE Transactions on*, 27(1):57–70, 2004.

[27] D. Saraswat, R. Achar, and M. S. Nakhla. Global passivity enforcement algorithm for macromodels of interconnect subnetworks characterized by tabulated data. *Very Large Scale Integration (VLSI) Systems, IEEE Transactions on*, 13(7):819–832, 2005.

[28] A. Semlyen and B. Gustavsen. A half-size singularity test matrix for fast and reliable passivity assessment of rational models. *Power Delivery, IEEE Transactions on*, 24(1):345–351, 2009.

[29] Kin Cheong Sou, A. Megretski, and L. Daniel. A quasi-convex optimization approach to parameterized model order reduction. *Computer-Aided Design of Integrated Circuits and Systems, IEEE Transactions on*, 27(3):456–469, 2008.

[30] Tatjana Stykel. Gramian-based model reduction for descriptor systems. *Math.Control Signals Systems Mathematics of Control, Signals and Systems*, 16(4):297–319, 2004. ID: 5648432313.

[31] P. Triverio, S. Grivet-Talocia, M. S. Nakhla, F. G. Canavero, and R. Achar. Stability, causality, and passivity in electrical interconnect models. *Advanced Packaging, IEEE Transactions on*, 30(4):795–808, 2007.

[32] Yuanzhe Wang, Chi-Un Lei, G. K. H. Pang, and Ngai Wong. Mfti: Matrix-format tangential interpolation for modeling multi-port systems. In *Design Automation Conference (DAC), 2010 47th ACM/IEEE*, pages 683–686, 2010.

[33] Yuanzhe Wang, Zheng Zhang, Cheng-Kok Koh, G. K. H. Pang, and Ngai Wong. Peds: Passivity enforcement for descriptor systems via hamiltonian-symplectic matrix pencil perturbation. In *Computer-Aided Design (ICCAD), 2010 IEEE/ACM International Conference on*, pages 800–807, 2010.

[34] Yuanzhe Wang, Zheng Zhang, Cheng-Kok Koh, Guoyong Shi, G. K. H. Pang, and Ngai Wong. Passivity enforcement for descriptor systems via matrix pencil perturbation. *Computer-Aided Design of Integrated Circuits and Systems, IEEE Transactions on*, 31(4):532–545, 2012.

[35] M. Ronald Wohlers. *Lumped and distributed passive networks; a generalized and advanced viewpoint*. Academic Press, New York, 1969.

[36] D. C. Youla, L. Castriota, and H. J. Carlin. Bounded real scattering matrices and the foundations of linear passive network theory. *Circuit Theory, IRE Transactions on*, 6(1):102–124, 1959.

[37] Zheng Zhang and Ngai Wong. An efficient projector-based passivity test for descriptor systems. *Computer-Aided Design of Integrated Circuits and Systems, IEEE Transactions on*, 29(8):1203–1214, 2010.

[38] Zheng Zhang and Ngai Wong. Passivity check of s-parameter descriptor systems via s-parameter generalized hamiltonian methods. *Advanced Packaging, IEEE Transactions on*, 33(4):1034–1042, 2010.